

Low Rank Quaternion Matrix Completion Based on Quaternion QR Decomposition and Sparse Regularizer

Juan Han^a, Liqiao Yang^a, Kit Ian Kou^{*a}, Jifei Miao^b, and Lizhi Liu^c

^aDepartment of Mathematics, Faculty of Science and Technology, University of Macau, Macau 999078, China

^bSchool of Mathematics and Statistics, Yunnan University, Kunming, Yunnan, 650091, China

^cDepartment of Radiology, Sun Yat-sen University Cancer Center, State Key Laboratory of Oncology in South China, Collaborative Innovation Center for Cancer Medicine, Guangdong Key Laboratory of Nasopharyngeal Carcinoma Diagnosis and Therapy, 651 Dongfeng Road East, Guangzhou, Guangdong, 510060, China

Abstract

Matrix completion is one of the most challenging problems in computer vision. Recently, quaternion representations of color images have achieved competitive performance in many fields. Because it treats the color image as a whole, the coupling information between the three channels of the color image is better utilized. Due to this, low-rank quaternion matrix completion (LRQMC) algorithms have gained considerable attention from researchers. In contrast to the traditional quaternion matrix completion algorithms based on quaternion singular value decomposition (QSVD), we propose a novel method based on quaternion QR decomposition (QQR). In the first part of the paper, a novel method for calculating an approximate QSVD based on iterative QQR is proposed (CQSVD-QQR), whose computational complexity is lower than that of QSVD. The largest r ($r > 0$) singular values of a given quaternion matrix can be computed by using CQSVD-QQR. Then, we propose a new quaternion matrix completion method based on CQSVD-QQR which combines low-rank and sparse priors of color images. Experimental results on color images and color medical images demonstrate that our model outperforms those state-of-the-art methods.

Keywords: quaternion matrix completion; quaternion QR decomposition; low rank; sparse representation

1 Introduction

Image completion, which aims to recover lost entries based on limited known pixels of an image, has a wide range of applications in computer vision. It has received extensive attention from researchers in recent years [1–4]. Low-rank matrix minimization problems are constructed and solved using low-rank properties of matrices. There has been great success with low-rank matrix completion (LRMC)-based methods. The low-rank property of LRMC-based methods is generally controlled by a constrained rank minimization problem. Let $\mathbf{M} \in \mathbb{R}^{M \times N}$, $M \geq N > 0$ be an incomplete matrix, and then the traditional LRMC-based method can be formulated as follows:

$$\min_{\mathbf{X}} \text{rank}(\mathbf{X}), \text{ s.t., } P_{\Omega}(\mathbf{X} - \mathbf{M}) = \mathbf{0}, \quad (1)$$

where $\mathbf{X} \in \mathbb{R}^{M \times N}$ is a completed output matrix, $\text{rank}(\cdot)$ is the rank function, and Ω is the observed entries set. $P_{\Omega}(\mathbf{X})$ is defined as

$$(P_{\Omega}(\mathbf{X}))_{mn} = \begin{cases} \mathbf{X}_{mn}, & (m, n) \in \Omega, \\ 0, & (m, n) \notin \Omega. \end{cases}$$

*Corresponding author: kikou@umac.mo

However, the rank function is discontinuous and non-convex, making it NP-hard. The nuclear norm has been shown to be the tightest convex relaxation of the above rank minimization problem [5]. Thus, the nuclear norm as a convex surrogate of the rank function is frequently used to deal with the image completion problem [6, 7]. The corresponding minimization method is formulated as

$$\min_{\mathbf{X}} \|\mathbf{X}\|_*, \text{ s.t., } P_{\Omega}(\mathbf{X} - \mathbf{M}) = \mathbf{0}, \quad (2)$$

However, the authors in [1] stated that these existing methods based on nuclear norm minimization minimize all singular values simultaneously, so the rank may not be well approximated. And they proposed the truncated nuclear norm (TNN) regularization, which approximates the rank function more accurately than the nuclear norm. Gu *et al.* [3, 8] introduced a weighted nuclear norm (WNNM) technique that gives different weights to singular values in order to treat them differently. Additionally, there are other enhanced nuclear norm-based approaches that have shown good image completion outcomes, such as [9–11].

When processing color images, the aforementioned LRMC-based approaches essentially process the RGB's three color channels individually before combining them to get the final restoration outcome. The loss of coupling information between the three color channels could result from this strategy's disregard for the relationships between the three channels.

Researchers have paid close attention to the quaternion representation of color images in recent years. Numerous studies have demonstrated the effectiveness of quaternions in describing color images, and techniques based on them have produced competitive outcomes for a variety of image processing issues, including color image edge identification [12], color face recognition [13], color image denoising [14], color image completion [4]. For a color image, its three color channels exactly match the three imaginary sections of a quaternion matrix. A pixel of a color image can be represented by a pure quaternion as follows:

$$\dot{p} = 0 + p_R i + p_G j + p_B k,$$

where \dot{p} denotes a color pixel, p_R , p_G , and p_B are the pixel values of the three channels RGB of \dot{p} , respectively, and i , j , k are the three imaginary units of a quaternion. The relationship between the three channels can be better leveraged since the pure quaternion matrix represents the three color channels of the color image holistically. Recently, approaches for image completion using quaternion-based LRMC have also been proposed. Similar to the problem (2), the widely used low-rank quaternion matrix completion algorithm (LRQMC) is formulated as follows:

$$\min_{\dot{\mathbf{X}}} \|\dot{\mathbf{X}}\|_*, \text{ s.t., } P_{\Omega}(\dot{\mathbf{X}} - \dot{\mathbf{M}}) = \mathbf{0}, \quad (3)$$

where $\dot{\mathbf{X}} \in \mathbb{H}^{M \times N}$ is the recovered output quaternion matrix, $\dot{\mathbf{M}} \in \mathbb{H}^{M \times N}$ is the observed quaternion matrix, and $\|\dot{\mathbf{X}}\|_*$ is the nuclear norm of a quaternion matrix $\dot{\mathbf{X}}$. $P_{\Omega}(\dot{\mathbf{X}})$ is defined as

$$(P_{\Omega}(\dot{\mathbf{X}}))_{mn} = \begin{cases} \dot{\mathbf{X}}_{mn}, & (m, n) \in \Omega, \\ 0, & (m, n) \notin \Omega. \end{cases}$$

Chen *et al.* [15] provided a general model for low-rank quaternion matrix completion based on the nuclear norm and three nonconvex rank surrogates (i.e., functions based on the Laplace function, Geman function, and weighted Schatten norm, respectively). These techniques can produce better results when compared to some traditional LRMC-based techniques. However, to use these techniques, one must first solve the quaternion singular value decomposition (QSVD) of the complete quaternion matrix, just as some other conventional LRMC-based techniques. Large processing matrices necessitate complex algorithms that take a long time to complete. Therefore, it would be wise to look into more effective algorithms. Three LRQMC approaches are suggested in [16] based on the quaternion double Frobenius norm (Q-DFN), quaternion double nuclear norm (Q-DNN), and quaternion Frobenius/nuclear norm (Q-FNN) minimization models. This algorithm only needs to process two-factor quaternion matrices of lesser sizes after these three quaternion-based bilinear factorizations of the quaternion matrix, which lessens the computing difficulty of solving the QSVD. However, this factorization might become entangled in local minima [17].

Furthermore, more information [18, 19] should be taken into account for improved image completion rather than just relying on the low-rank qualities of images. The image completion problem can be

impacted significantly by the sparsity of images in a particular domain, such as transform domains where many signals have a naturally sparse structure. To provide an approach for image completion, the authors [20] combined low-rank and sparse priors. The l_1 -norm regularizer is used to formulate the sparse prior, and the truncated nuclear norm is chosen as the surrogate of the rank function. The authors in [21] extended this method to the quaternion system. These methods can achieve relatively good completion results but still rely on the QSVD calculation of large matrices.

Actually, singular values and singular vectors can also be calculated by Qatar Riyal (QR) decomposition [19]. Inspired by this, in this paper, we propose a novel quaternion Tri-Factorization method and thus we only need to calculate the QSVD of a small quaternion matrix. We also take the sparsity into account to increase the accuracy of the completion results. The main contributions of this paper are summarized as follows:

- A novel method for calculating an approximate QSVD (CQSVD-QQR) is proposed based on quaternion Qatar Riyal decomposition (QQR). The suggested approach can compute the largest $r(r > 0)$ singular values of a given quaternion matrix, and its computational complexity is lower than QSVD's.
- Based on the novel quaternion Tri-Factorization method and sparse quaternion matrix priors, we propose a novel LRQMC model. The dimension of the quaternion matrix in the quaternion nuclear norm regularization term is reduced based on CQSVD-QQR.

Listed below is the organization of this article. In Section 2, numerous notations are introduced along with a brief overview of the fundamentals of quaternion algebra. Section 3 of the paper provides a brief discussion of the theory of the quaternion discrete cosine transform. The CQSVD-QQR technique for computing an approximate QSVD, which is based on the quaternion QR decomposition, is then given. After that our proposed quaternion-based matrix completion algorithm, QQR-QNN-SR is introduced. We also discuss the computational complexities of QQR-QNN-SR. In Section 4, we illustrate the convergence of CQSVD-QQR and provide some examples of our method's utility in real-world situations. We also compare our method with some state-of-the-art methods. The conclusion is presented in Section 5.

2 Notations and preliminaries

This section begins with a summary of various mathematical notations and ends with a brief review of some fundamental quaternion algebra concepts. In addition, we recommend [22] for a more comprehensive understanding of quaternion algebra.

2.1 Notations

In this paper, we use \mathbb{R} , \mathbb{C} , \mathbb{H} to present the set of real numbers, the set of complex numbers, and the set of quaternions, respectively. In real and complex fields, scalars, vectors, and matrices are indicated by lowercase letters, such as, a , boldface lowercase letters, such as, \mathbf{a} , and boldface capital letters, such as, \mathbf{A} , respectively. The symbols \dot{q} , $\dot{\mathbf{q}}$, $\dot{\mathbf{Q}}$, respectively, stand for a quaternion scalar, vector, and matrix, respectively. The symbols $(\cdot)^{-1}$, $(\cdot)^\dagger$, $(\cdot)^T$, $(\cdot)^*$, and $(\cdot)^H$, respectively, stand for the inverse, pseudoinverse, transpose, conjugation, and conjugate transpose. The identity matrix is represented by $\mathbf{I}_m \in \mathbb{R}^{m \times m}$.

2.2 Basic knowledge of quaternion algebra

Quaternion was introduced by W.R. Hamilton [23] in 1843. A quaternion $\dot{q} \in \mathbb{H}$ can be represented as follows:

$$\dot{q} = q_0 + q_1 i + q_2 j + q_3 k,$$

where $q_0, q_1, q_2, q_3 \in \mathbb{R}$, and i, j, k are imaginary number units which obey the following multiplication rules:

$$\begin{cases} i^2 = j^2 = k^2 = ijk = -1, \\ ij = -ji = k, jk = -kj = i, ki = -ik = j. \end{cases}$$

We can rewrite a quaternion $\dot{q} = q_0 + q_1i + q_2j + q_3k$ as $\dot{q} = q_0 + q_1i + (q_2 + q_3i)j = c_1 + c_2j$, where $c_1, c_2 \in \mathbb{C}$. A quaternion $\dot{q} \in \mathbb{H}$ can also be decomposed into a real part $\Re(\dot{q})$ and a vector part $\mathbf{V}(\dot{q})$ as follows:

$$\dot{q} = \Re(\dot{q}) + \mathbf{V}(\dot{q}),$$

where $\Re(\dot{q}) = q_0 \in \mathbb{R}$, and $\mathbf{V}(\dot{q}) = q_1i + q_2j + q_3k$. Moreover, if $\Re(\dot{q}) = 0$, then \dot{q} is called a pure quaternion. And $\mathbf{V}(\mathbb{H})$ denotes the set of pure quaternions.

The conjugate of a quaternion is given by $\dot{q}^* = q_0 - q_1i - q_2j - q_3k$. And the norm of a quaternion is defined as $|\dot{q}| = \sqrt{q\dot{q}^*} = \sqrt{q^*q} = \sqrt{q_0^2 + q_1^2 + q_2^2 + q_3^2}$. It is worth noting that the commutative law of multiplication on the quaternion system does not hold, i.e., $\dot{q}_1\dot{q}_2 \neq \dot{q}_2\dot{q}_1$ in general.

Similarly, Let $\dot{\mathbf{Q}} = (\dot{q}_{mn}) \in \mathbb{H}^{M \times N}$ be a quaternion matrix, then $\dot{\mathbf{Q}} = \mathbf{Q}_0 + \mathbf{Q}_1i + \mathbf{Q}_2j + \mathbf{Q}_3k$, where $\mathbf{Q}_t \in \mathbb{R}^{M \times N}$ ($t = 0, 1, 2, 3$). A quaternion matrix is named a pure quaternion matrix, if $\Re(\dot{\mathbf{Q}}) = \mathbf{Q}_0 = \mathbf{0}$.

The Frobenius norm of a quaternion matrix $\dot{\mathbf{Q}}$ is defined as: $\|\dot{\mathbf{Q}}\|_F = \sqrt{\sum_{m=1}^M \sum_{n=1}^N |\dot{q}_{mn}|^2} = \sqrt{\text{tr}(\dot{\mathbf{Q}}^H \dot{\mathbf{Q}})}$. And the nuclear norm of $\dot{\mathbf{Q}}$ is defined as: $\|\dot{\mathbf{Q}}\|_* = \sum_t \sigma_t$, where σ_t is the nonzero singular value of $\dot{\mathbf{Q}}$.

Definition 1 (The complex representation of a quaternion matrix [24]). Given a quaternion matrix $\dot{\mathbf{Q}} = \mathbf{Q}_0 + \mathbf{Q}_1i + \mathbf{Q}_2j + \mathbf{Q}_3k \in \mathbb{H}^{M \times N}$, it can be written as $\dot{\mathbf{Q}} = \mathbf{Q}_a + \mathbf{Q}_bj$, which is called the Cayley-Dickson form of $\dot{\mathbf{Q}}$. And the complex representation of $\dot{\mathbf{Q}}$ is defined as follows

$$\chi_{\dot{\mathbf{Q}}} = \begin{bmatrix} \mathbf{Q}_a & \mathbf{Q}_b \\ -\mathbf{Q}_b^* & \mathbf{Q}_a^* \end{bmatrix}, \quad (4)$$

where $\mathbf{Q}_a = \mathbf{Q}_0 + \mathbf{Q}_1i$, $\mathbf{Q}_b = \mathbf{Q}_2 + \mathbf{Q}_3i \in \mathbb{C}^{M \times N}$, $\mathbf{Q}_a^* = \mathbf{Q}_0 - \mathbf{Q}_1i$, $\mathbf{Q}_b^* = \mathbf{Q}_2 - \mathbf{Q}_3i$, and $\chi_{\dot{\mathbf{Q}}} \in \mathbb{C}^{2M \times 2N}$.

The complex representation matrices of quaternions and associated matrices share a number of characteristics. We suggest reading [24] for more details.

Theorem 1 (Singular value decomposition of a quaternion matrix (QSVD) [24]). Given a quaternion matrix $\dot{\mathbf{Q}} \in \mathbb{H}^{M \times N}$ of rank r , there exist two quaternion unitary matrices $\dot{\mathbf{U}} \in \mathbb{H}^{M \times M}$ and $\dot{\mathbf{V}} \in \mathbb{H}^{N \times N}$ such that

$$\dot{\mathbf{Q}} = \dot{\mathbf{U}} \begin{bmatrix} \Sigma_r & \mathbf{0} \\ \mathbf{0} & \mathbf{0} \end{bmatrix} \dot{\mathbf{V}}^H = \dot{\mathbf{U}} \Lambda \dot{\mathbf{V}}^H, \quad (5)$$

where Σ_r is a real diagonal matrix with r positive singular values of $\dot{\mathbf{Q}}$ on its diagonal.

Theorem 2 (The quaternion Qar Riyal decomposition (QQR) [25]). Given any quaternion matrix $\dot{\mathbf{A}} \in \mathbb{H}^{M \times N}$ of rank r , there exist a unitary matrix $\dot{\mathbf{Q}} \in \mathbb{H}^{M \times M}$ and a weakly upper triangular quaternion matrix $\dot{\mathbf{R}} \in \mathbb{H}^{M \times N}$ such that

$$\dot{\mathbf{A}} = \dot{\mathbf{Q}} \dot{\mathbf{R}}. \quad (6)$$

That is, there exists a permutation matrix $\mathbf{P} \in \mathbb{R}^{N \times N}$ such that $\dot{\mathbf{R}}\mathbf{P}$ is an upper triangular quaternion matrix.

3 Our method of quaternion completion

3.1 Quaternion discrete cosine transform

In this section, we give a brief introduction to the quaternion discrete cosine transform.

Definition 2 (Forward quaternion discrete cosine transform (FQDCT) [26]). Since quaternions do not satisfy commutativity, quaternion discrete cosine transform (QDCT) of a quaternion matrix $\dot{\mathbf{Q}} \in \mathbb{H}^{M \times N}$ has two forms [26], i.e., left-handed form and right-handed form:

$$FQDCT^L(u, v) = \alpha(u)\alpha(v) \sum_{m=0}^{M-1} \sum_{n=0}^{N-1} \dot{q} \dot{\mathbf{Q}}(m, n) N(u, v, m, n), \quad (7)$$

$$FQDCT^R(u, v) = \alpha(u)\alpha(v) \sum_{m=0}^{M-1} \sum_{n=0}^{N-1} \dot{\mathbf{Q}}(m, n) N(u, v, m, n) \dot{q}, \quad (8)$$

where $\Re(\dot{q}) = 0$ named a quaternionization factor and satisfies $\dot{q}^2 = -1$. Similar to discrete cosine transform (DCT) in the real domain, $\alpha(u)$, $\alpha(v)$, and $N(u, v, m, n)$ take the values

$$\alpha(u) = \begin{cases} \sqrt{\frac{1}{M}} & \text{for } u = 0 \\ \sqrt{\frac{2}{M}} & \text{for } u \neq 0 \end{cases}, \quad \alpha(v) = \begin{cases} \sqrt{\frac{1}{N}} & \text{for } v = 0 \\ \sqrt{\frac{2}{N}} & \text{for } v \neq 0 \end{cases}, \quad (9)$$

$$N(u, v, m, n) = \cos \left[\frac{\pi(2m+1)u}{2M} \right] \cos \left[\frac{\pi(2n+1)v}{2N} \right]. \quad (10)$$

According to the FQDCT, the form of inverse quaternion discrete cosine transform (IQDCT) also has two categories, which are given as follows:

$$IQDCT^L(m, n) = \sum_{u=0}^{M-1} \sum_{v=0}^{N-1} \alpha(u) \alpha(v) \dot{q} \dot{\mathbf{C}}(u, v) N(u, v, m, n), \quad (11)$$

$$IQDCT^R(m, n) = \sum_{u=0}^{M-1} \sum_{v=0}^{N-1} \alpha(u) \alpha(v) \dot{\mathbf{C}}(u, v) N(u, v, m, n) \dot{q}, \quad (12)$$

where $\dot{\mathbf{C}} \in \mathbb{H}^{M \times N}$.

Theorem 3 (The relationship between FQDCT and IQDCT [26]).

$$\begin{aligned} \dot{\mathbf{Q}}(m, n) &= IQDCT^L \left[FQDCT^L(\dot{\mathbf{Q}}(m, n)) \right] \\ &= IQDCT^R \left[FQDCT^R(\dot{\mathbf{Q}}(m, n)) \right]. \end{aligned} \quad (13)$$

The computation technique for $FQDCT^L$, which may be summed up as the following steps [26], is used to establish our suggested model, thus we only briefly discuss it here.

1. Given a quaternion matrix $\dot{\mathbf{Q}}(m, n) \in \mathbb{H}^{M \times N}$, write it in its Cayley-Dickson form, i.e., $\dot{\mathbf{Q}}(m, n) = \mathbf{Q}_a(m, n) + \mathbf{Q}_b(m, n)j$, where $\mathbf{Q}_a(m, n)$ and $\mathbf{Q}_b(m, n) \in \mathbb{C}^{M \times N}$.
2. Calculate the DCT of $\mathbf{Q}_a(m, n)$ and $\mathbf{Q}_b(m, n)$, and the corresponding results are written as $DCT(\mathbf{Q}_a(m, n))$, and $DCT(\mathbf{Q}_b(m, n))$, respectively.
3. Forming a quaternion matrix from $DCT(\mathbf{Q}_a(m, n))$, and $DCT(\mathbf{Q}_b(m, n))$, which is given by $\dot{\mathbf{Q}}(m, n) = DCT(\mathbf{Q}_a(m, n)) + DCT(\mathbf{Q}_b(m, n))j$.
4. The final result is given by multiplying $\dot{\mathbf{Q}}$ by the quaternionization factor \dot{q} :

$$FQDCT^L \left[\dot{\mathbf{Q}}(m, n) \right] = \dot{q} \dot{\mathbf{Q}}(m, n).$$

3.2 A new method for computing an approximate QSVD based on quaternion QR decomposition (CQSVD-QQR)

Assume that $\dot{\mathbf{X}} \in \mathbb{H}^{M \times N}$ is a given quaternion matrix. In this section, we propose a method for computing the largest r ($r \in (0, N]$) singular values and associated singular vectors of $\dot{\mathbf{X}}$ by using QQR decomposition, named CQSVD-QQR. In this method, $\dot{\mathbf{X}}$ is decomposed into three quaternion matrices, $\dot{\mathbf{L}} \in \mathbb{H}^{M \times r}$, $\dot{\mathbf{D}} \in \mathbb{H}^{r \times r}$, $\dot{\mathbf{R}} \in \mathbb{H}^{r \times N}$, such that

$$\left\| \dot{\mathbf{X}} - \dot{\mathbf{L}} \dot{\mathbf{D}} \dot{\mathbf{R}} \right\|_F^2 \leq \varepsilon, \quad (14)$$

where ε represents a positive tolerance. Therefore, we can formulate a quaternion minimization problem

$$\min_{\dot{\mathbf{L}}, \dot{\mathbf{D}}, \dot{\mathbf{R}}} \left\| \dot{\mathbf{X}} - \dot{\mathbf{L}} \dot{\mathbf{D}} \dot{\mathbf{R}} \right\|_F^2, \quad \text{s.t., } \dot{\mathbf{L}}^H \dot{\mathbf{L}} = \mathbf{I}_r, \quad \dot{\mathbf{R}} \dot{\mathbf{R}}^H = \mathbf{I}_r, \quad (15)$$

As can be shown from (15), for three variables $\dot{\mathbf{L}}$, $\dot{\mathbf{D}}$, and $\dot{\mathbf{R}}$, the minimization function is convex to the third variable when two of them are arbitrarily fixed. As a result, we can update these three variables sequentially. The results of the three variables in the τ th iteration are denoted as $\dot{\mathbf{L}}^\tau$, $\dot{\mathbf{D}}^\tau$, and $\dot{\mathbf{R}}^\tau$, respectively. Let $\dot{\mathbf{L}}^1 = \text{eye}(M, r)$, $\dot{\mathbf{D}}^1 = \text{eye}(r, r)$, and $\dot{\mathbf{R}}^1 = \text{eye}(r, N)$. By fixing $\dot{\mathbf{D}}^\tau$ and $\dot{\mathbf{R}}^\tau$, $\dot{\mathbf{L}}^{\tau+1}$ can be updated by solving the following problem

$$\dot{\mathbf{L}}^{\tau+1} = \arg \min_{\dot{\mathbf{L}}} \left\| \dot{\mathbf{X}} - \dot{\mathbf{L}} \dot{\mathbf{D}}^\tau \dot{\mathbf{R}}^\tau \right\|_F^2, \quad (16)$$

It can be easily verified that the optimal solution to (16) is given by

$$\dot{\mathbf{L}}^{\tau+1} = \dot{\mathbf{X}}(\dot{\mathbf{R}}^\tau)^H(\dot{\mathbf{D}}^\tau)^\dagger, \quad (17)$$

where $(\dot{\mathbf{D}}^\tau)^\dagger$ is the quaternionic pseudoinverse of $\dot{\mathbf{D}}^\tau$. According to (15), the optimal $\dot{\mathbf{L}}$ is a column orthogonal quaternion matrix, so $\dot{\mathbf{L}}^{\tau+1}$ can be chosen as the orthogonal basis of the range space spanned by the columns of $\dot{\mathbf{X}}(\dot{\mathbf{R}}^\tau)^H(\dot{\mathbf{D}}^\tau)^\dagger$, that is,

$$\dot{\mathbf{L}}^{\tau+1} = \text{orth}(\dot{\mathbf{X}}(\dot{\mathbf{R}}^\tau)^H(\dot{\mathbf{D}}^\tau)^\dagger), \quad (18)$$

where $\text{orth}(\dot{\mathbf{X}})$ represents an operator that computes the orthogonal basis of the columns of $\dot{\mathbf{X}}$. From (14), it is clear that $\dot{\mathbf{L}}^{\tau+1}$ is the orthogonal basis for the range of $\dot{\mathbf{X}}$. And $\dot{\mathbf{L}}^{\tau+1}$ can be computed as the orthogonal basis of $\dot{\mathbf{X}}\dot{\mathbf{\Omega}}$, where $\dot{\mathbf{\Omega}} \in \mathbb{H}^{N \times r}$ is a quaternion random matrix [27]. Thus, $\dot{\mathbf{L}}^{\tau+1}$ can be computed as follows:

$$\dot{\mathbf{L}}^{\tau+1} = \text{orth}(\dot{\mathbf{X}}(\dot{\mathbf{R}}^\tau)^H). \quad (19)$$

Like the method CSVD-QR in the real domain [19], quaternion QR decomposition is also used to calculate the orthogonal basis of $\dot{\mathbf{X}}(\dot{\mathbf{R}}^\tau)^H$. $\dot{\mathbf{L}}^{\tau+1}$ is given by

$$[\dot{\mathbf{Q}}, \dot{\mathbf{S}}] = \text{QQR}(\dot{\mathbf{X}}(\dot{\mathbf{R}}^\tau)^H), \quad (20)$$

$$\dot{\mathbf{L}}^{\tau+1} = \dot{\mathbf{Q}}(\mathbf{q}_1, \dots, \mathbf{q}_r), \quad (21)$$

where $\dot{\mathbf{Q}} \in \mathbb{H}^{M \times M}$ and $\dot{\mathbf{S}} \in \mathbb{H}^{M \times r}$, and $\text{QQR}(\dot{\mathbf{X}})$ is an operator that computes the quaternion QR decomposition of $\dot{\mathbf{X}}$. Thus, it can be seen from (20) that $\dot{\mathbf{X}}(\dot{\mathbf{R}}^\tau)^H = \dot{\mathbf{Q}}\dot{\mathbf{S}}$. Similarly, $\dot{\mathbf{R}}^{\tau+1}$ is updated as follows:

$$[\dot{\mathbf{G}}, \dot{\mathbf{T}}] = \text{QQR}(\dot{\mathbf{X}}^H \dot{\mathbf{L}}^{\tau+1}), \quad (22)$$

$$\dot{\mathbf{R}}^{\tau+1} = \dot{\mathbf{G}}(\mathbf{q}_1, \dots, \mathbf{q}_r), \quad (23)$$

where $\dot{\mathbf{G}} \in \mathbb{H}^{N \times N}$ and $\dot{\mathbf{T}} \in \mathbb{H}^{N \times r}$, and $\dot{\mathbf{X}}^H \dot{\mathbf{L}}^{\tau+1} = \dot{\mathbf{G}}\dot{\mathbf{T}}$. In view of (15), the optimal $\dot{\mathbf{R}}$ is a row orthogonal quaternion matrix, which can be set as follows:

$$\dot{\mathbf{R}}^{\tau+1} = (\dot{\mathbf{R}}^{\tau+1})^H. \quad (24)$$

With fixing the values of $\dot{\mathbf{L}}^{\tau+1}$ and $\dot{\mathbf{R}}^{\tau+1}$, $\dot{\mathbf{D}}^{\tau+1}$ can be updated by solving the following optimization problem:

$$\dot{\mathbf{D}} = \arg \min_{\dot{\mathbf{D}}} \left\| \dot{\mathbf{X}} - \dot{\mathbf{L}}^{\tau+1} \dot{\mathbf{D}} \dot{\mathbf{R}}^{\tau+1} \right\|_F^2, \quad (25)$$

Since $(\dot{\mathbf{L}}^{\tau+1})^H \dot{\mathbf{L}}^{\tau+1} = \mathbf{I}_r$, $\dot{\mathbf{R}}^{\tau+1}(\dot{\mathbf{R}}^{\tau+1})^H = \mathbf{I}_r$, it is easy to prove that the optimal solution to (25) is as follows:

$$\dot{\mathbf{D}}^{\tau+1} = (\dot{\mathbf{L}}^{\tau+1})^H \dot{\mathbf{X}}(\dot{\mathbf{R}}^{\tau+1})^H. \quad (26)$$

Since $\dot{\mathbf{X}}^H \dot{\mathbf{L}}^{\tau+1} = \dot{\mathbf{G}}\dot{\mathbf{T}}$, we can get that

$$\dot{\mathbf{T}}^H = (\dot{\mathbf{L}}^{\tau+1})^H \dot{\mathbf{X}} \dot{\mathbf{G}}. \quad (27)$$

According to (23) and (24) for updating $\dot{\mathbf{R}}^{\tau+1}$, we have

$$\dot{\mathbf{D}}^{\tau+1} = \dot{\mathbf{T}}^H(1 \dots r, 1 \dots r), \quad (28)$$

The three sequences $\{\dot{\mathbf{L}}^{\tau+1}\}$, $\{\dot{\mathbf{R}}^{\tau+1}\}$, and $\{\dot{\mathbf{D}}^{\tau+1}\}$ ($\tau = 1, \dots, n, \dots$) obtained by (21), (24), and (28) can converge to quaternion matrices $\dot{\mathbf{L}}$, $\dot{\mathbf{R}}$, and $\dot{\mathbf{D}}$, respectively. And $\dot{\mathbf{D}}$ satisfies

$$\|\dot{\mathbf{D}}_{ss}\|_1 = \|\Lambda_{ss}\|_1, \quad (29)$$

where $s = 1, \dots, r$ and Λ_{ss} is the s th singular value of $\dot{\mathbf{X}}$. In the next subsection, we will use the output of CQSVD-QQR with one iteration to initialize the date of our proposed quaternion matrix completion model.

Table 1: Computing an approximate QSVD based on quaternion QR decomposition (CQSVD-QQR).

Input:	The quaternion matrix $\dot{\mathbf{X}} \in \mathbb{H}^{M \times N}$.
1:	Initialize $r > 0$; $\tau = 1$; $\varepsilon > 0$; $\text{It}_{\max} > 0$; $\dot{\mathbf{L}}^1 = \text{eye}(M, r)$; $\dot{\mathbf{D}}^1 = \text{eye}(r, r)$; $\dot{\mathbf{R}}^1 = \text{eye}(r, N)$.
2:	Repeat
3:	$\dot{\mathbf{L}}^{\tau+1}$: (20 - 21).
4:	$\dot{\mathbf{R}}^{\tau+1}$: (22 - 24).
5:	$\dot{\mathbf{D}}^{\tau+1}$: (22, 28).
6:	Until convergence: $\ \dot{\mathbf{L}}^\tau \dot{\mathbf{D}}^\tau \dot{\mathbf{R}}^\tau - \dot{\mathbf{X}}\ _F^2 \leq \varepsilon$ or $\tau > \text{It}_{\max}$.
Output:	$\dot{\mathbf{L}}^{t+1}$, $\dot{\mathbf{D}}^{t+1}$, $\dot{\mathbf{R}}^{t+1}$.

3.3 Proposed quaternion-based methods for color image completion

This section presents the formulation of the proposed method.

lemma 1. Given quaternion matrices $\dot{\mathbf{L}} \in \mathbb{H}^{M \times r}$, $\dot{\mathbf{R}} \in \mathbb{H}^{r \times N}$, and $\dot{\mathbf{D}} \in \mathbb{H}^{r \times r}$, and assume that $\dot{\mathbf{L}}$ and $\dot{\mathbf{R}}$ have orthogonal columns and orthogonal rows, respectively, i.e., $\dot{\mathbf{L}}^H \dot{\mathbf{L}} = \mathbf{I}_r$, $\dot{\mathbf{R}}(\dot{\mathbf{R}})^H = \mathbf{I}_r$, then $\|\dot{\mathbf{D}}\|_* = \|\dot{\mathbf{L}}\dot{\mathbf{D}}\dot{\mathbf{R}}\|_*$.

Proof. The QSVD of $\dot{\mathbf{D}}$ can be obtained by using Theorem 1 as follows:

$$\dot{\mathbf{D}} = \dot{\mathbf{U}} \begin{bmatrix} \Sigma_s & \mathbf{0} \\ \mathbf{0} & \mathbf{0} \end{bmatrix} \dot{\mathbf{V}}^H = \dot{\mathbf{U}}_s \Sigma_s \dot{\mathbf{V}}_s^H, \quad (30)$$

where $\dot{\mathbf{U}}_s \in \mathbb{H}^{r \times s}$ and $\dot{\mathbf{V}}_s \in \mathbb{H}^{r \times s}$ satisfy $\dot{\mathbf{U}}_s^H \dot{\mathbf{U}}_s = \mathbf{I}_s$ and $\dot{\mathbf{V}}_s^H \dot{\mathbf{V}}_s = \mathbf{I}_s$, respectively, $\Sigma_s = \text{diag}(\sigma_1, \sigma_2, \dots, \sigma_s) \in \mathbb{H}^{s \times s}$ contains the s positive singular values of $\dot{\mathbf{D}}$, and $s \leq r$. Thus, we have

$$\dot{\mathbf{L}}\dot{\mathbf{D}}\dot{\mathbf{R}} = \dot{\mathbf{L}}\dot{\mathbf{U}}_s \Sigma_s \dot{\mathbf{V}}_s^H \dot{\mathbf{R}} = \dot{\mathbf{L}}\dot{\mathbf{U}}_s \Sigma_s (\dot{\mathbf{R}}^H \dot{\mathbf{V}}_s)^H. \quad (31)$$

It can be checked that $(\dot{\mathbf{L}}\dot{\mathbf{U}}_s)^H \dot{\mathbf{L}}\dot{\mathbf{U}}_s = \mathbf{I}_s$, and $(\dot{\mathbf{R}}^H \dot{\mathbf{V}}_s)^H \dot{\mathbf{R}}^H \dot{\mathbf{V}}_s = \mathbf{I}_s$. Therefore, it can be found that (31) is one of the SVDs of $\dot{\mathbf{L}}\dot{\mathbf{D}}\dot{\mathbf{R}}$. And $\|\dot{\mathbf{D}}\|_* = \sum_{t=1}^s \sigma_t = \|\dot{\mathbf{L}}\dot{\mathbf{D}}\dot{\mathbf{R}}\|_*$. \square

Quaternion nuclear norm minimization is a well-established and potent strategy among all models for quaternion-based completion. It can be viewed as the generalization of the nuclear norm minimization of the real matrix. Lemma 1 allows us to determine that $\|\dot{\mathbf{X}}\|_* = \|\dot{\mathbf{L}}\dot{\mathbf{D}}\dot{\mathbf{R}}\|_* = \|\dot{\mathbf{D}}\|_*$. Substituting $\dot{\mathbf{X}} = \dot{\mathbf{L}}\dot{\mathbf{D}}\dot{\mathbf{R}}$ into the original quaternion nuclear norm minimization problem, we can formulate the new model as follows:

$$\min_{\dot{\mathbf{L}}, \dot{\mathbf{D}}, \dot{\mathbf{R}}} \|\dot{\mathbf{D}}\|_*, \text{ s.t.}, \begin{cases} \dot{\mathbf{L}}^H \dot{\mathbf{L}} = \mathbf{I}_r, \dot{\mathbf{R}}\dot{\mathbf{R}}^H = \mathbf{I}_r, \\ \dot{\mathbf{X}} = \dot{\mathbf{L}}\dot{\mathbf{D}}\dot{\mathbf{R}}, P_\Omega(\dot{\mathbf{L}}\dot{\mathbf{D}}\dot{\mathbf{R}} - \dot{\mathbf{M}}) = \mathbf{0}. \end{cases} \quad (32)$$

As we previously stated, the color image completion problem cannot be solved by just taking into account the image's low-rank prior information. To address it, we, therefore, integrate the image's low-rank prior with its sparseness in a transform domain. By introducing sparsity, we can obtain the following model:

$$\min_{\dot{\mathbf{L}}, \dot{\mathbf{D}}, \dot{\mathbf{R}}} \|\dot{\mathbf{D}}\|_* + \lambda \|\dot{\mathbf{W}}\|_1, \text{ s.t.}, \begin{cases} \dot{\mathbf{L}}^H \dot{\mathbf{L}} = \mathbf{I}_r, \dot{\mathbf{R}}\dot{\mathbf{R}}^H = \mathbf{I}_r, \\ \dot{\mathbf{X}} = \dot{\mathbf{L}}\dot{\mathbf{D}}\dot{\mathbf{R}}, P_\Omega(\dot{\mathbf{X}} - \dot{\mathbf{L}}\dot{\mathbf{D}}\dot{\mathbf{R}}) = \mathbf{0}, \mathcal{T}(\dot{\mathbf{X}}) = \dot{\mathbf{W}}, \end{cases} \quad (33)$$

where $\mathcal{T}(\cdot)$ represents the transform operator, $\dot{\mathbf{W}} = \mathcal{T}(\dot{\mathbf{X}})$ is the transformed quaternion matrix, and the parameter $\lambda > 0$. Specifically, we use the FQDCT^L to establish the model, so the operator $\mathcal{T}(\dot{\mathbf{X}})$ here refers to the FQDCT^L of $\dot{\mathbf{X}}$. Since this formulation employs a method for approximating QSVD based on quaternion QR decomposition (CQSVD-QR), quaternion nuclear norm, and a sparse regularizer, we name the proposed method as QQR-QNN-SR.

3.4 Optimization framework

The optimization problem (33) is addressed in this section using the alternating direction method of multipliers (ADMM) framework. This framework in the quaternion system is similar to the ADMM

framework in the complex number field [28]. The augmented Lagrangian function of the problem (33) is given by

$$\begin{aligned}
\mathcal{L}(\dot{\mathbf{X}}, \dot{\mathbf{L}}, \dot{\mathbf{D}}, \dot{\mathbf{R}}, \dot{\mathbf{W}}, \dot{\mathbf{Y}}, \dot{\mathbf{Z}}) \\
= \|\dot{\mathbf{D}}\|_* + \lambda \|\dot{\mathbf{W}}\|_1 \\
+ \Re(\langle \dot{\mathbf{Y}}, \dot{\mathbf{X}} - \dot{\mathbf{L}}\dot{\mathbf{D}}\dot{\mathbf{R}} \rangle) + \frac{\mu}{2} \|\dot{\mathbf{X}} - \dot{\mathbf{L}}\dot{\mathbf{D}}\dot{\mathbf{R}}\|_F^2 \\
+ \Re(\langle \dot{\mathbf{Z}}, \dot{\mathbf{W}} - \mathcal{T}(\dot{\mathbf{X}}) \rangle) + \frac{\mu}{2} \|\dot{\mathbf{W}} - \mathcal{T}(\dot{\mathbf{X}})\|_F^2,
\end{aligned} \tag{34}$$

where the penalty parameter $\mu > 0$, $\dot{\mathbf{Y}}$ and $\dot{\mathbf{Z}}$ are Lagrange multiplier. The optimization problem (33) can have each parameter updated alternatively by fixing other variables, in accordance with the ADMM framework. Particularly, all variables can be updated iteratively as follows:

$$\begin{cases}
\dot{\mathbf{L}}^{t+1} = \arg \min_{\dot{\mathbf{L}}} \mathcal{L}(\dot{\mathbf{X}}^t, \dot{\mathbf{L}}, \dot{\mathbf{D}}^t, \dot{\mathbf{R}}^t, \dot{\mathbf{W}}^t, \dot{\mathbf{Y}}^t, \dot{\mathbf{Z}}^t), \\
\dot{\mathbf{R}}^{t+1} = \arg \min_{\dot{\mathbf{R}}} \mathcal{L}(\dot{\mathbf{X}}^t, \dot{\mathbf{L}}^{t+1}, \dot{\mathbf{D}}^t, \dot{\mathbf{R}}, \dot{\mathbf{W}}^t, \dot{\mathbf{Y}}^t, \dot{\mathbf{Z}}^t), \\
\dot{\mathbf{D}}^{t+1} = \arg \min_{\dot{\mathbf{D}}} \mathcal{L}(\dot{\mathbf{X}}^t, \dot{\mathbf{L}}^{t+1}, \dot{\mathbf{D}}, \dot{\mathbf{R}}^{t+1}, \dot{\mathbf{W}}^t, \dot{\mathbf{Y}}^t, \dot{\mathbf{Z}}^t), \\
\dot{\mathbf{X}}^{t+1} = \arg \min_{\dot{\mathbf{X}}} \mathcal{L}(\dot{\mathbf{X}}, \dot{\mathbf{L}}^{t+1}, \dot{\mathbf{D}}^{t+1}, \dot{\mathbf{R}}^{t+1}, \dot{\mathbf{W}}^t, \dot{\mathbf{Y}}^t, \dot{\mathbf{Z}}^t), \\
\dot{\mathbf{W}}^{t+1} = \arg \min_{\dot{\mathbf{W}}} \mathcal{L}(\dot{\mathbf{X}}^{t+1}, \dot{\mathbf{L}}^{t+1}, \dot{\mathbf{D}}^{t+1}, \dot{\mathbf{R}}^{t+1}, \dot{\mathbf{W}}, \dot{\mathbf{Y}}^t, \dot{\mathbf{Z}}^t), \\
\dot{\mathbf{Y}}^{t+1} = \dot{\mathbf{Y}}^t + \mu^t (\dot{\mathbf{X}}^{t+1} - \dot{\mathbf{L}}^{t+1} \dot{\mathbf{D}}^{t+1} \dot{\mathbf{R}}^{t+1}), \\
\dot{\mathbf{Z}}^{t+1} = \dot{\mathbf{Z}}^t + \mu^t (\dot{\mathbf{W}}^{t+1} - \mathcal{T}(\dot{\mathbf{X}}^{t+1})).
\end{cases} \tag{35}$$

As shown in (35), we first fix other variables to solve the corresponding optimization problem to update $\dot{\mathbf{L}}$, $\dot{\mathbf{D}}$, and $\dot{\mathbf{R}}$.

Updating $\dot{\mathbf{L}}$, $\dot{\mathbf{D}}$, and $\dot{\mathbf{R}}$: In the $t + 1$ -th iteration, $\dot{\mathbf{L}}^{t+1}$ and $\dot{\mathbf{R}}^{t+1}$ are updated by solving the following minimization problem:

$$\min_{\dot{\mathbf{L}}, \dot{\mathbf{R}}} \left\| \left(\dot{\mathbf{X}}^t + \frac{\dot{\mathbf{Y}}^t}{\mu^t} \right) - \dot{\mathbf{L}} \dot{\mathbf{D}}^t \dot{\mathbf{R}} \right\|_F^2. \tag{36}$$

According to the analysis of the quaternion optimization problem (15), $\dot{\mathbf{L}}$, and $\dot{\mathbf{R}}$ can be obtained by using CQSVD-QQR as follows:

$$\begin{cases}
[\dot{\mathbf{L}}^{t+1}, \sim] = \text{QQR}((\dot{\mathbf{X}}^t + \frac{\dot{\mathbf{Y}}^t}{\mu^t})(\dot{\mathbf{R}}^t)^H), \\
\dot{\mathbf{L}}^{t+1} = \dot{\mathbf{L}}^{t+1}(\mathbf{q}_1, \dots, \mathbf{q}_r),
\end{cases} \tag{37}$$

and

$$\begin{cases}
[\dot{\mathbf{R}}^{t+1}, \dot{\mathbf{D}}^t] = \text{QQR}((\dot{\mathbf{X}}^t + \frac{\dot{\mathbf{Y}}^t}{\mu^t})^H \dot{\mathbf{L}}^{t+1}), \\
\dot{\mathbf{R}}^{t+1} = (\dot{\mathbf{R}}^{t+1}(\mathbf{q}_1, \dots, \mathbf{q}_r))^H,
\end{cases} \tag{38}$$

where QQR is the quaternion QR decomposition. If the two variables $\dot{\mathbf{L}}$ and $\dot{\mathbf{R}}$ are started as $\dot{\mathbf{L}}^t$ and $\dot{\mathbf{R}}^t$, the CQSVD-QQR method will converge within a limited number of iterations because the quaternion matrices $\dot{\mathbf{L}}$ and $\dot{\mathbf{R}}$ will not change significantly in two consecutive iterations. As a result, in the proposed method for quaternion matrix completion, the output of CQSVD-QQR with one iteration is used. In one iteration of CQSVD-QQR, this method decomposes the quaternion matrix $\dot{\mathbf{X}}^t + \frac{\dot{\mathbf{Y}}^t}{\mu^t}$ as follows:

$$\dot{\mathbf{X}}^t + \frac{\dot{\mathbf{Y}}^t}{\mu^t} = \dot{\mathbf{L}}^{t+1} \hat{\dot{\mathbf{D}}}^t \dot{\mathbf{R}}^{t+1}, \tag{39}$$

where $\hat{\dot{\mathbf{D}}}^t = \dot{\mathbf{D}}^t(1 \dots r, 1 \dots r) \in \mathbb{H}^{r \times r}$. According to (15) and (39), we also have

$$\hat{\dot{\mathbf{D}}}^t = (\dot{\mathbf{L}}^{t+1})^H (\dot{\mathbf{X}}^t + \frac{\dot{\mathbf{Y}}^t}{\mu^t}) (\dot{\mathbf{R}}^{t+1})^H. \tag{40}$$

After updating $\dot{\mathbf{L}}$ and $\dot{\mathbf{R}}$, we can update $\dot{\mathbf{D}}$ by solving the following problem:

$$\dot{\mathbf{D}}^{t+1} = \arg \min_{\dot{\mathbf{D}}} \|\dot{\mathbf{D}}\|_* + \frac{\mu^t}{2} \|\dot{\mathbf{D}} - (\dot{\mathbf{L}}^{t+1})^H (\dot{\mathbf{X}}^t + \frac{\dot{\mathbf{Y}}^t}{\mu^t}) (\dot{\mathbf{R}}^{t+1})^H\|_F^2, \quad (41)$$

Substituting (40) into (41), then the above problem can be reformulated as follows:

$$\dot{\mathbf{D}}^{t+1} = \arg \min_{\dot{\mathbf{D}}} \|\dot{\mathbf{D}}\|_* + \frac{\mu^t}{2} \|\dot{\mathbf{D}} - \hat{\dot{\mathbf{D}}}^t\|_F^2. \quad (42)$$

The closed solution to the problem (42) is [15]

$$\dot{\mathbf{D}}^{t+1} = \mathcal{D}_{\frac{1}{\mu^t}}(\hat{\dot{\mathbf{D}}}^t) = \dot{\mathbf{U}} \mathcal{S}_{\frac{1}{\mu^t}}(\Sigma) \dot{\mathbf{V}}^H, \quad (43)$$

where $\hat{\dot{\mathbf{D}}}^t = \dot{\mathbf{U}} \Sigma \dot{\mathbf{V}}^H$ is the QSVD of $\dot{\mathbf{D}}^t$, and $\mathcal{S}_{\frac{1}{\mu^t}}(\Sigma) = \text{diag}(\max\{\sigma_p(\hat{\dot{\mathbf{D}}}^t) - \frac{1}{\mu^t}, 0\})$ is the soft thresholding operator, and $\sigma_p(\hat{\dot{\mathbf{D}}}^t)$ is the p -th positive singular value of $\hat{\dot{\mathbf{D}}}^t$.

Updating $\dot{\mathbf{X}}$, $\dot{\mathbf{W}}$, $\dot{\mathbf{Y}}$, $\dot{\mathbf{Z}}$, and μ : In the $t+1$ -th iteration, fixing the variables $\dot{\mathbf{L}}^{t+1}$, $\dot{\mathbf{D}}^{t+1}$, $\dot{\mathbf{R}}^{t+1}$, $\dot{\mathbf{X}}^{t+1}$ is the optimal solution of the problem as follows:

$$\begin{aligned} \dot{\mathbf{X}}^{t+1} &= \arg \min_{\dot{\mathbf{X}}} \Re(\langle \dot{\mathbf{Y}}^t, \dot{\mathbf{X}} - \dot{\mathbf{L}}^{t+1} \dot{\mathbf{D}}^{t+1} \dot{\mathbf{R}}^{t+1} \rangle) + \frac{\mu^t}{2} \|\dot{\mathbf{X}} - \dot{\mathbf{L}}^{t+1} \dot{\mathbf{D}}^{t+1} \dot{\mathbf{R}}^{t+1}\|_F^2 \\ &\quad + \Re(\langle \dot{\mathbf{Z}}^t, \dot{\mathbf{W}}^t - \mathcal{T}(\dot{\mathbf{X}}) \rangle) + \frac{\mu^t}{2} \|\dot{\mathbf{W}}^t - \mathcal{T}(\dot{\mathbf{X}})\|_F^2, \\ &= \arg \min_{\dot{\mathbf{X}}} \frac{\mu^t}{2} \|\dot{\mathbf{X}} + \frac{\dot{\mathbf{Y}}^t}{\mu^t} - \dot{\mathbf{L}}^{t+1} \dot{\mathbf{D}}^{t+1} \dot{\mathbf{R}}^{t+1}\|_F^2 + \frac{\mu^t}{2} \|\dot{\mathbf{W}}^t + \frac{\dot{\mathbf{Z}}^t}{\mu^t} - \mathcal{T}(\dot{\mathbf{X}})\|_F^2. \end{aligned} \quad (44)$$

Because the existence of the term $\mathcal{T}(\dot{\mathbf{X}})$ in problem (44), the variable $\dot{\mathbf{X}}$ cannot be directly separated from the other variables. Fortunately, the Parseval theorem in the quaternion system isolates the variable $\dot{\mathbf{X}}$ from the operator $\mathcal{T}(\cdot)$, allowing us to reformulate the issue. Similar to the real domain, the Parseval theorem in the quaternion system [29] asserts that the total energy of the signal remains unchanged after a unitary transformation, such as quaternion discrete Fourier transform (QDFT), and quaternion discrete cosine transform (QDCT). Therefore, by introducing the corresponding inverse transform to the last term of (44), we have

$$\|\dot{\mathbf{W}}^t + \frac{\dot{\mathbf{Z}}^t}{\mu^t} - \mathcal{T}(\dot{\mathbf{X}})\|_F^2 = \|\mathcal{I}_{\mathcal{T}}(\dot{\mathbf{W}}^t + \frac{\dot{\mathbf{Z}}^t}{\mu^t}) - \dot{\mathbf{X}}\|_F^2, \quad (45)$$

where $\mathcal{I}_{\mathcal{T}}(\cdot)$ is the inverse transform of $\mathcal{T}(\cdot)$. After substituting (45) into (44) and ignoring terms unrelated to the variable $\dot{\mathbf{X}}$, the optimization problem used to update $\dot{\mathbf{X}}$ can be written as follows

$$\dot{\mathbf{X}}^{t+1} = \arg \min_{\dot{\mathbf{X}}} \left\| \frac{1}{2} (\dot{\mathbf{L}}^{t+1} \dot{\mathbf{D}}^{t+1} \dot{\mathbf{R}}^{t+1} - \frac{\dot{\mathbf{Y}}^t}{\mu^t} + \mathcal{I}_{\mathcal{T}}(\dot{\mathbf{W}}^t + \frac{\dot{\mathbf{Z}}^t}{\mu^t})) - \dot{\mathbf{X}} \right\|_F^2. \quad (46)$$

Thus, we can obtain that

$$\dot{\mathbf{X}}^{t+1} = \frac{1}{2} (\dot{\mathbf{L}}^{t+1} \dot{\mathbf{D}}^{t+1} \dot{\mathbf{R}}^{t+1} - \frac{\dot{\mathbf{Y}}^t}{\mu^t} + \mathcal{I}_{\mathcal{T}}(\dot{\mathbf{W}}^t + \frac{\dot{\mathbf{Z}}^t}{\mu^t})). \quad (47)$$

Combined with the constraint that $P_{\Omega}(\dot{\mathbf{L}} \dot{\mathbf{D}} \dot{\mathbf{R}}) = P_{\Omega}(\dot{\mathbf{M}})$, the value of $\dot{\mathbf{X}}$ should remain unchanged on the observed entries set Ω , i.e.,

$$\dot{\mathbf{X}}^{t+1} = P_{\Omega^c}(\dot{\mathbf{X}}^{t+1}) + P_{\Omega}(\dot{\mathbf{M}}), \quad (48)$$

where Ω^c is the set of locations corresponding to missing entries.

Next, in the $t+1$ -th iteration, the variable $\dot{\mathbf{W}}^{t+1}$ is updated by solving the following problem:

$$\begin{aligned} \dot{\mathbf{W}}^{t+1} &= \arg \min_{\dot{\mathbf{W}}} \lambda \|\dot{\mathbf{W}}\|_1 + \Re(\langle \dot{\mathbf{Z}}^t, \dot{\mathbf{W}} - \mathcal{T}(\dot{\mathbf{X}}^{t+1}) \rangle) + \frac{\mu^t}{2} \|\dot{\mathbf{W}} - \mathcal{T}(\dot{\mathbf{X}}^{t+1})\|_F^2 \\ &= \arg \min_{\dot{\mathbf{W}}} \lambda \|\dot{\mathbf{W}}\|_1 + \frac{\mu^t}{2} \|\dot{\mathbf{W}} + \frac{\dot{\mathbf{Z}}^t}{\mu^t} - \mathcal{T}(\dot{\mathbf{X}}^{t+1})\|_F^2. \end{aligned} \quad (49)$$

Table 2: The QQR-QNN-SR-based quaternion matrix completion method.

Input: The observed quaternion matrix data $\dot{\mathbf{M}} \in \mathbb{H}^{M \times N}$ with $\mathcal{P}_{\Omega^c}(\dot{\mathbf{M}}) = \mathbf{0}$; λ ; μ_{\max} ; γ and $r > 0$.

1: **Initialize** $t = 0$; μ^0 ; $\varepsilon > 0$; $\text{It}_{\max} > 0$; $\dot{\mathbf{L}}^0 = \text{eye}(M, r)$; $\dot{\mathbf{R}}^0 = \text{eye}(r, N)$; $\dot{\mathbf{D}}^0 = \text{eye}(r, r)$; $\dot{\mathbf{X}}^0 = \dot{\mathbf{M}}$; $\dot{\mathbf{W}}^0 = \mathbf{0}$.

2: **Repeat**

3: **Step 1.** $\dot{\mathbf{L}}^{t+1}$, $\dot{\mathbf{R}}^{t+1}$: (37) and (38), respectively.

4: **Step 2.** $\dot{\mathbf{D}}^{t+1} = \mathcal{D}_{\frac{1}{\mu^t}}(\dot{\mathbf{D}}^t) = \dot{\mathbf{U}} \mathcal{S}_{\frac{1}{\mu^t}}(\Sigma) \dot{\mathbf{V}}^H$.

5: **Step 3.** $\dot{\mathbf{X}}^{t+1} = \mathcal{P}_{\Omega^c}(\frac{1}{2}(\dot{\mathbf{L}}^{t+1} \dot{\mathbf{D}}^{t+1} \dot{\mathbf{R}}^{t+1} - \frac{\dot{\mathbf{Y}}^t}{\mu^t} + \mathcal{T}(\dot{\mathbf{W}}^t + \frac{\dot{\mathbf{Z}}^t}{\mu^t})) + \mathcal{P}_{\Omega}(\dot{\mathbf{M}})$.

6: **Step 4.** $\dot{\mathbf{W}}^{t+1} = \mathcal{S}_{\frac{4\lambda}{\mu^t}}(\mathcal{T}(\dot{\mathbf{X}}^{t+1}) - \frac{\dot{\mathbf{Z}}^t}{\mu^t})$.

7: $\dot{\mathbf{Y}}^{t+1} = \dot{\mathbf{Y}}^t + \mu^t(\dot{\mathbf{X}}^{t+1} - \dot{\mathbf{L}}^{t+1} \dot{\mathbf{D}}^{t+1} \dot{\mathbf{R}}^{t+1})$.

8: $\dot{\mathbf{Z}}^{t+1} = \dot{\mathbf{Z}}^t + \mu^t(\dot{\mathbf{W}}^{t+1} - \mathcal{T}(\dot{\mathbf{X}}^{t+1}))$.

9: $\mu^{t+1} = \min(\gamma \mu^t, \mu_{\max})$.

10: **Until convergence**

Output: $\dot{\mathbf{L}}^{t+1}$, $\dot{\mathbf{D}}^{t+1}$, $\dot{\mathbf{R}}^{t+1}$, $\dot{\mathbf{X}}^{t+1}$, and $\dot{\mathbf{W}}^{t+1}$.

The optimal solution to (49) is

$$\dot{\mathbf{W}}^{t+1} = \mathcal{S}_{\frac{4\lambda}{\mu^t}}(\mathcal{T}(\dot{\mathbf{X}}^{t+1}) - \frac{\dot{\mathbf{Z}}^t}{\mu^t}), \quad (50)$$

where $\mathcal{S}_p(\dot{\mathbf{x}}) = \frac{\dot{\mathbf{x}}}{|\dot{\mathbf{x}}|} \max\{|\dot{\mathbf{x}}| - p, 0\}$ is the element-wise soft thresholding operator [21].

Finally, the variables $\dot{\mathbf{Y}}^{t+1}$, $\dot{\mathbf{Z}}^{t+1}$, and the penalty parameter μ^{t+1} are updated as follows:

$$\dot{\mathbf{Y}}^{t+1} = \dot{\mathbf{Y}}^t + \mu^t(\dot{\mathbf{X}}^{t+1} - \dot{\mathbf{L}}^{t+1} \dot{\mathbf{D}}^{t+1} \dot{\mathbf{R}}^{t+1}), \quad (51)$$

$$\dot{\mathbf{Z}}^{t+1} = \dot{\mathbf{Z}}^t + \mu^t(\dot{\mathbf{W}}^{t+1} - \mathcal{T}(\dot{\mathbf{X}}^{t+1})), \quad (52)$$

and

$$\mu^{t+1} = \gamma \mu^t. \quad (53)$$

The whole procedure of the proposed method is summarized in Table 2.

3.5 Complexity analysis

In this section, we analyze the computational complexity of the proposed QQR-QNN-SR method. As shown in Table 2, the main computational cost of each iteration of QQR-QNN-SR involves the update cost of two types of variables, one is the cost of updating variables $\dot{\mathbf{L}}$, $\dot{\mathbf{D}}$, and $\dot{\mathbf{R}}$, and the other is the cost of updating variables $\dot{\mathbf{X}}$ and $\dot{\mathbf{W}}$. The complexity when updating variables of the first type is dominated by the quaternion QR decomposition operation of two quaternion matrices of size $M \times r$ and $N \times r$ whose complexity is about $\mathcal{O}(r^2(M + N) - r^3)$, and the calculation of the QSVD of an $r \times r$ quaternion matrix whose complexity is about $\mathcal{O}(r^3)$, where $r < \min\{M, N\}$. However, methods directly based on the quaternion nuclear norm, such as LRQA-G [15], need to calculate the QSVD of the quaternion matrix with size $M \times N$, and the complexity is about $\mathcal{O}(\min(MN^2, M^2N))$. It is clear that the computational cost of QR decomposition of two quaternion matrices of size $M \times r$ and $N \times r$ is smaller than that of QSVD of the quaternion matrix with size $M \times N$. In the second part of QQR-QNN-SR, the computational complexity is dominated by the transform operator \mathcal{T} . And the complexity is about $\mathcal{O}(M^2N^2 + MN)$. Therefore, the total computational complexity of each iteration of the proposed QQR-QNN-SR method is dominated by the second part with the complexity being about $\mathcal{O}(M^2N^2 + MN)$.

4 Experimental results and discussion

In this section, we first give a test of the convergence of CQSVD-QQR. The effectiveness of the proposed QQR-QNN-SR method is then demonstrated by conducting numerical experiments on color images.

We perform all the experiments on a MATLAB 2019b platform equipped with an i7-9700 CPU and 16 GB of RAM.

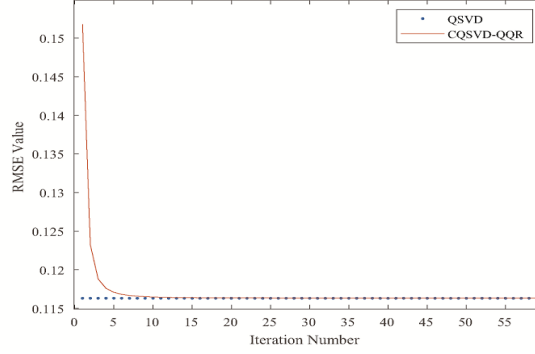


Fig. 1. Comparison of RMSE values of CQSVD-QQR and QSVD.



Fig. 2. Convergence procedure of $\dot{\mathbf{D}}_\tau$ in CQSVD-QQR. (a) $k = 5$. (b) $k = 20$. (c) $k = 40$. (d) $k = 60$.

4.1 Convergence of CQSVD-QQR

First, a synthetic quaternion matrix $\dot{\mathbf{X}}$ is generated as follows:

$$\dot{\mathbf{X}} = \dot{\mathbf{M}}_1^{m \times r_1} \dot{\mathbf{M}}_2^{r_1 \times n}, \quad (54)$$

where $r_1 \in [1, n]$ is the rank of $\dot{\mathbf{X}}$, and $\dot{\mathbf{M}}_1^{m \times r_1}$ and $\dot{\mathbf{M}}_2^{r_1 \times n}$ are two quaternion random matrices. Then, let $m = n = 300$, $r_1 = 250$, $r = 120$, with the largest r singular values. Firstly, we use the proposed CQSVD-QQR to obtain the quaternion Tri-Factorization of $\dot{\mathbf{X}}$. And we compare the results using the root-mean-square error (RMSE), which is defined as

$$\text{RMSE} = \sqrt{\frac{\|\dot{\mathbf{X}} - \dot{\mathbf{Y}}\|_F^2}{mn}}, \quad (55)$$

where $\dot{\mathbf{X}}, \dot{\mathbf{Y}} \in \mathbb{H}^{m \times n}$, $\dot{\mathbf{X}}$ is the original data, and $\dot{\mathbf{Y}}$ is the reconstructed result. After that, RMSE for the model CQSVD-QQR with respect to the variable $\dot{\mathbf{X}}_{\text{LDR}}$ can be obtained. Similarly, we can calculate RMSE for the model QSVD with respect to \mathbf{X}_{QSVD} , where $\dot{\mathbf{X}}_{\text{LDR}}$ and \mathbf{X}_{QSVD} denote the reconstructed results of CQSVD-QQR and QSVD, respectively.

As shown in Fig. 1 that CQSVD-QQR will converge to a certain value as the number of iterations increases. Moreover, the accuracy of CQSVD-QQR is close to that of the QSVD method after a few iterative steps.

Additionally, the variable $\dot{\mathbf{D}}_\tau$ in CQSVD-QQR will converge to a diagonal matrix. Let $\dot{\mathbf{T}}_\tau \in \mathbb{R}^{r \times r}$ be a square matrix with each element $\dot{\mathbf{T}}_\tau(u, v) = |\dot{\mathbf{D}}_\tau(u, v)|$, for $i, j = 1, \dots, r$. In order to demonstrate the convergence of $\dot{\mathbf{D}}_\tau$, we compute $\dot{\mathbf{D}}_5$, $\dot{\mathbf{D}}_{20}$, $\dot{\mathbf{D}}_{40}$, and $\dot{\mathbf{D}}_{60}$. And the convergence can be shown by plotting $10\dot{\mathbf{T}}_\tau$ ($\tau = 5, 20, 40, 60$), as shown in Fig. 2.

4.2 Experimental results of QQR-QNN-SR

This section tests the proposed QQR-QNN-SR utilizing several natural color images and color medical images. We perform numerical experiments to complete (quaternion) matrices with random missing entries and matrices with random block missing entries. The ratio of the missing entries (MR)

ranges from a minimum of 50% to a maximum of 90% to better demonstrate the efficacy of our technique.

Compared method: We compare the proposed QQR-QNN-SR with several state-of-the-art completion methods, including IRLNM-QR [19], WNNM [3], MC-NC [30], TNNR [1], TNN-SR [20], LRQMC [4], LRQA-G [15], QLNF [21], TQLNA [21]. The first five methods are real matrix-based completion algorithms, and the last four are low-rank completion algorithms based on quaternion matrices.

Quantitative assessment and natural color image for testing: To evaluate the performance of the proposed QQR-QNN-SR, we use two commonly used measures, including peak signal-to-noise ratio (PSNR), and the structure similarity (SSIM). Higher PSNR and SSIM indicate better recovery performance. Among all the methods compared, the best numerical results are bolded.

Eight widely used natural color images with size 256×256 in Fig. 3 are selected as the test images in our experiments. Like the processing in [20], among all the methods compared, those based on real matrix completion first process the three color channels separately, and then combine the results of the three channels to obtain the final result.

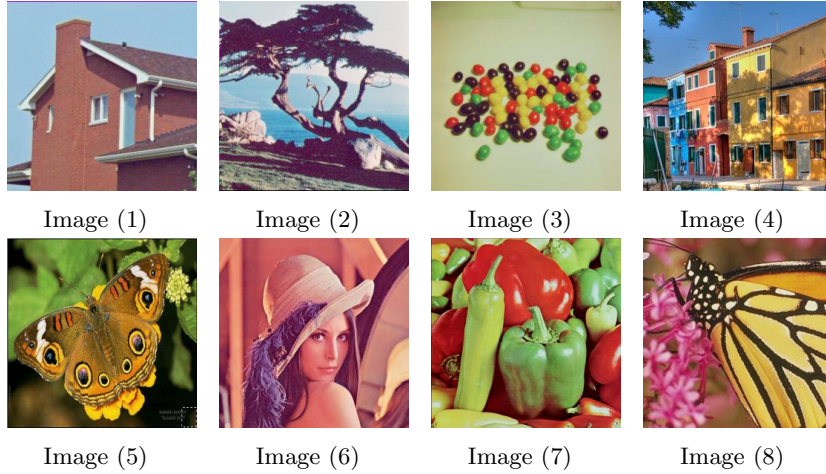


Fig. 3. The 8 color images with size $256 \times 256 \times 3$.

Simulations with different parameters of QQR-QNN-SR: Since the settings of parameters λ , μ^0 , r are closely related to the performance of the proposed method, we investigate the influence of different values of these parameters on the recovery results within a certain range of values.

Firstly, the settings of $\mu^0 = \{10^{-4}, 5 \times 10^{-4}, 10^{-3}, 5 \times 10^{-3}, 10^{-2}, 5 \times 10^{-2}, 10^{-1}, 5 \times 10^{-1}, 10^0, 10^1, 10^2\}$ are tested with other parameters ($\lambda = 10^{-1}$, $r = 85$, $\gamma = 1.15$) fixed. The results for the eight color images are shown in Fig. 4. After comprehensively considering the recovery results under the different missing ratios of pixels, it can be found from Fig. 4 that the proper settings of μ^0 are between $[10^{-2}, 10^{-1}]$, and the best value of μ^0 is 5×10^{-2} .

Secondly, by fixing the values of λ , μ^0 , and γ to $\lambda = 10^{-1}$, $\mu^0 = 5 \times 10^{-2}$, and $\gamma = 1.15$, the PSNR and SSIM values of the recovered images of the test images obtained by taking different values of r , where $r = \{5, 15, 25, 35, 45, 55, 65, 75, 85, 95, 105, 115, 125, 135, 150\}$, are shown in the Fig. 4. When the MR is larger, the value of r corresponding to the best recovery result is smaller. This is also in line with the fact that the larger the missing rate, the less original image information contained in the observed image, and the more low-rank the corresponding image is. Specifically, in the case of MR=50%, MR=70%, MR=80%, and MR=90%, the values of r that can obtain the best recovery results are 125, 85, 65, and 45, respectively.

Finally, set $\lambda = \{10^{-3}, 5 \times 10^{-3}, 10^{-2}, 5 \times 10^{-2}, 10^{-1}, 5 \times 10^{-1}, 10^0, 1.5 \times 10^0, 5 \times 10^0, 10^1, 10^2, 10^3\}$ and fix other parameters ($\mu^0 = 5 \times 10^{-2}$, $r = \{125, 65, 45\}$ correspond to MR = $\{50\%, 80\%, 90\%\}$, respectively, and $\gamma = 1.15$) to study the influence of the settings of parameter λ on performance of the results. The quantitatively evaluated results are shown in Fig. 4. It can be seen from Fig. 4 that when $\lambda \geq 10^{-1}$, the values of PSNR and SSIM no longer increase rapidly and tend to decrease slowly. We can see that relatively good results can be achieved when $\lambda = 10^{-1}$.

Experiments on natural color images: In this simulation, the proposed QQR-QNN-SR method

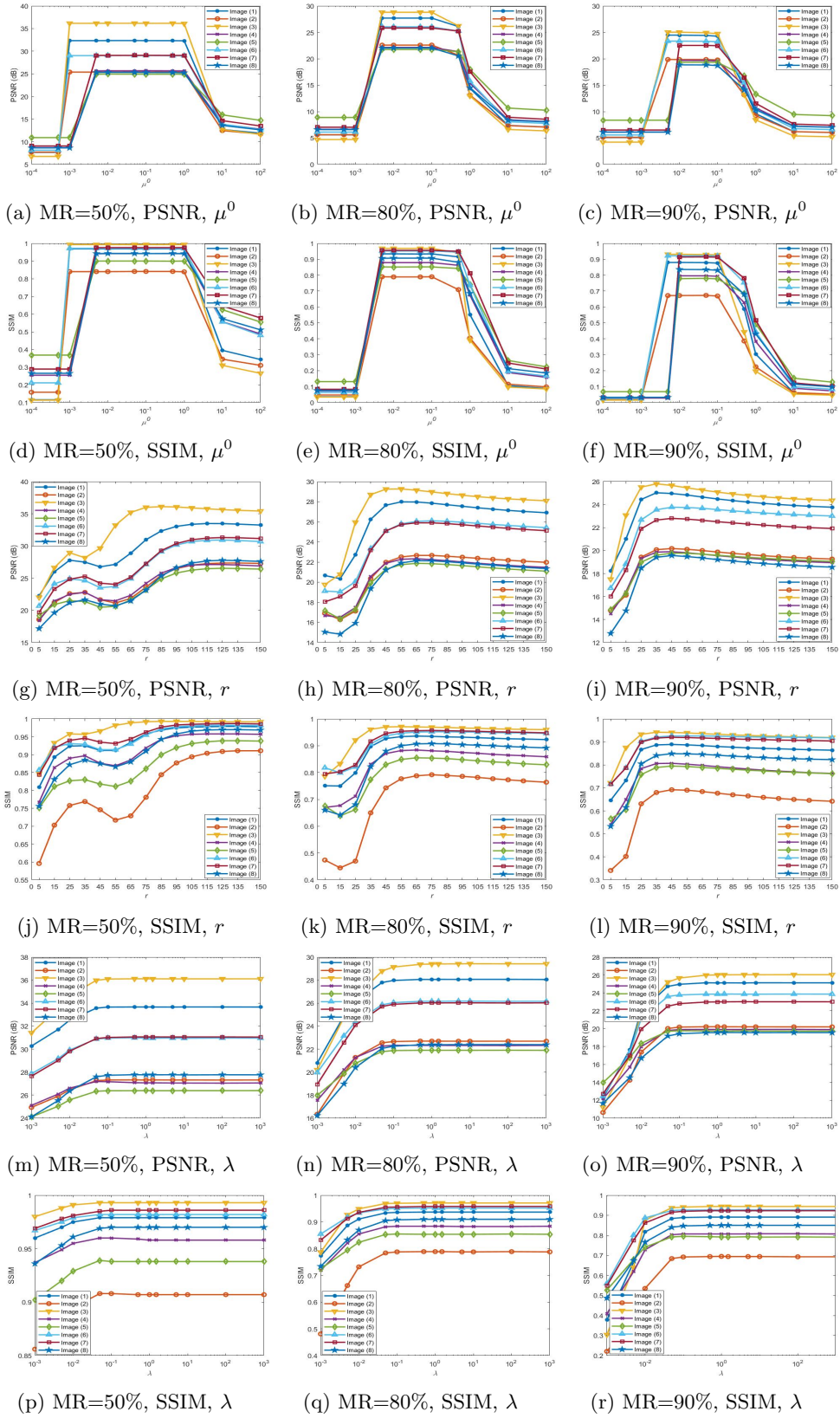


Fig. 4. (a)-(f) The PSNR values (in dB) and SSIM values obtained by the proposed QQR-QNN-SR method using different μ^0 's with $\lambda = 10^{-1}$ and $r = 85$. (g)-(l) The PSNR values (in dB) and SSIM values obtained by the proposed QQR-QNN-SR method using different r 's with $\lambda = 10^{-1}$ and $\mu^0 = 5 \times 10^{-2}$. (m)-(r) The PSNR values (in dB) and SSIM values obtained by the proposed QQR-QNN-SR method using different λ 's with $\mu^0 = 5 \times 10^{-2}$, $r = 125$ for MR=50%, $r = 65$ for MR=80%, and $r = 45$ for MR=90%.

was compared with several state-of-the-art completion methods. For QQR-QNN-SR, we set $\lambda = 10^{-1}$, $\mu^0 = 5 \times 10^{-2}$, $\gamma = 1.15$. And when $MR = \{90\%, 80\%, 70\%, 50\%\}$, r is correspondingly set as 45, 65, 85, and 125. The larger the value of MR , the more missing pixels. The higher the MR value is, the smaller the corresponding rank is.

The recovery results of different methods when $MR = 70\%$ and the corresponding quantitative evaluation results are shown in Fig. 5. As shown in Fig. 5, the proposed QQR-QNN-SR method not only achieves the best visual results but also the best quantitative results compared to other methods. Compared with other methods, the two methods TNN-SR and QQR-QNN-SR can achieve better completion results, which illustrates the importance of the sparse prior. And compared with method TNN-SR, the completion effect of method QQR-QNN-SR is better, which is mainly due to the superiority of quaternion to characterize color images. To better demonstrate the superiority of our proposed method, the visual results of Image (2) and Image (8) recovered by the QQR-QNN-SR method and several state-of-the-art methods when $MR = 90\%$ are shown in Fig. 6. Comparing the visual results recovered by our proposed method with those obtained by other state-of-the-art methods, it can be found that our method can recover more details of the original images.

Experiments on color medical images: Medical imaging technology has an irreplaceable role and wide application in clinical diagnosis. In the medical field, quaternion completion facilitates medical diagnosis based on medical images such as roentgen-ray computed tomography (CT), magnetic resonance imaging (MRI), single photon/positron emission computed tomography (SPECT/PET), and their overlay. For example, the medical color image recovery of the human brain based on quaternion completion methods can help doctors to better diagnose various brain diseases, such as Alzheimer’s disease (AD). Specifically, because AD often causes atrophy of the region of the hippocampus in patients, MRIs of their hippocampus may become blurred. In order to understand the degree of atrophy of the patient’s hippocampus, the patient’s healthy hippocampus data needs to be estimated and compared with the atrophic hippocampus data. Therefore, the MRI data of the hippocampus region completed by the quaternion completion method can better help doctors diagnose AD. Furthermore, recovering the data of specific regions of interest in medical images through the quaternion completion method can better help doctors diagnose diseases. In addition, due to equipment or human factors (such as patient body movements during medical examinations), the acquired medical image will be incomplete, which in turn affects the doctor’s diagnosis of the disease. Hence, quaternion completion can also be used to solve such problems.

In the experiments, the test images are eight color 256×256 medical images from the publicly available medical image database “The Whole Brain Atlas”¹ provided by Harvard Medical School. The eight color images are shown in Fig. 7. To more comprehensively verify the effectiveness of our method, we not only implement experiments with random missing with $MR = 90\%$ but also random block missing based on random block masks. For the random block missing, 2 random rhombus blocks of each image are masked, as shown in Fig. 8. And the lengths of the two diagonals of each rhombus are around 44 and 32.

In the experiment with $MR = 90\%$, the parameters of QQR-QNN-SR are set as $\lambda = 10^{-1}$, $\mu^0 = 5 \times 10^{-2}$, $\gamma = 1.15$, and $r = 45$. In the experiment with 2 random rhombus blocks missing, we set the parameters of QQR-QNN-SR as $\lambda = 5 \times 10^{-1}$, $\mu^0 = 5 \times 10^{-2}$, $\gamma = 1.6$, and $r = 190$. We compare the PSNR and SSIM values of the color medical images recovered by our method and IRLNM-QR, WNNM, MC-NC, TNNR, TNN-SR, LRQMC, LRQA-G, QLNF, and TQLNA, and the numerical results of different methods are shown in Fig. 7. Color medical images recovered by different methods are shown in Fig. 7 and Fig. 8. When $MR = 90\%$, improving the quality of recovered images is not a simple task. And as can be seen from the Fig. 7, our method achieves the highest PSNR and SSIM values in almost all recovered images compared to other methods. Additionally, Fig. 7 shows the visual advantage of our approach. Compared with recovering the images with random missing, recovering the images with the loss of random blocks is a more challenging problem to handle because the corruptions of the pixels are not evenly distributed and some important texture information contained in random blocks is lost as a whole. In such experiments, as can be seen from Fig. 8, compared with other methods, our method achieves competitive results both numerically and visually.

¹<http://www.med.harvard.edu/AANLIB/home.html>



Methods:	IRLNM-QR	WNNM	MC-NC	TNNR	TNN-SR	LRQMC	LRQA-G	QLNF	TQLNA	QQR-QNN-SR
MR = 50%										
Image (1)	27.701/0.938	27.919/0.922	29.703/0.957	30.171/0.953	33.276/0.978	30.221/0.960	30.107/0.958	24.308/0.858	30.867/0.959	33.470/0.979
Image (2)	23.481/0.842	22.099/0.732	25.470/0.880	24.873/0.812	25.484/0.903	25.374/0.873	24.992/0.858	19.622/0.604	25.378/0.823	27.351/0.909
Image (3)	27.308/0.955	29.334/0.962	30.277/0.974	31.115/0.975	35.482/0.992	31.183/0.979	31.064/0.978	24.664/0.916	31.965/0.980	35.636/0.992
Image (4)	23.610/0.915	22.298/0.884	25.296/0.940	25.068/0.934	26.664/0.955	25.567/0.942	25.169/0.936	19.976/0.800	25.594/0.940	27.113/0.958
Image (5)	23.243/0.888	21.235/0.808	24.292/0.897	24.003/0.877	26.013/0.926	24.399/0.912	24.132/0.901	19.822/0.766	24.426/0.882	26.538/0.939
Image (6)	26.135/0.956	25.027/0.932	27.804/0.967	27.784/0.964	30.686/0.982	28.083/0.968	27.773/0.966	22.660/0.911	28.121/0.966	30.922/0.983
Image (7)	25.178/0.949	25.019/0.944	27.989/0.972	27.656/0.969	30.663/0.985	28.434/0.975	27.779/0.970	21.415/0.890	28.483/0.974	31.307/0.987
Image (8)	22.125/0.906	21.271/0.874	24.617/0.940	24.041/0.929	27.471/0.969	24.338/0.938	24.158/0.934	18.013/0.796	24.529/0.935	27.888/0.971
Aver.	24.848	24.275	26.931	26.839	29.467	27.200	26.897	21.310	27.420	30.028
MR = 70%										
Image (1)	24.310/0.881	23.195/0.816	25.895/0.904	25.299/0.883	29.867/0.955	25.044/0.893	25.656/0.897	23.205/0.831	25.970/0.895	30.283/0.958
Image (2)	20.263/0.716	17.991/0.526	21.273/0.726	20.734/0.663	23.247/0.834	21.204/0.731	21.051/0.710	18.964/0.554	21.310/0.678	24.360/0.843
Image (3)	23.723/0.912	23.650/0.890	25.867/0.936	25.242/0.923	31.078/0.980	25.250/0.930	25.776/0.935	23.600/0.896	26.172/0.936	31.658/0.983
Image (4)	20.396/0.832	18.175/0.748	21.218/0.856	20.871/0.842	23.389/0.906	20.928/0.847	21.215/0.852	19.266/0.774	21.557/0.859	24.039/0.918
Image (5)	20.279/0.808	17.438/0.674	20.175/0.791	20.415/0.783	23.006/0.878	20.390/0.811	20.647/0.811	19.088/0.738	20.849/0.797	23.470/0.891
Image (6)	22.714/0.916	20.740/0.842	23.902/0.925	23.460/0.915	27.301/0.963	23.899/0.927	23.556/0.920	21.868/0.894	23.791/0.920	27.649/0.965
Image (7)	21.559/0.898	20.502/0.860	23.562/0.928	22.920/0.916	26.940/0.966	23.031/0.921	23.265/0.922	20.766/0.873	23.746/0.928	27.670/0.971
Image (8)	18.670/0.826	16.757/0.722	19.629/0.840	19.164/0.822	23.603/0.931	19.117/0.838	19.620/0.843	17.267/0.763	19.930/0.845	24.139/0.937
Aver.	21.489	19.806	22.690	22.263	26.054	22.358	22.598	20.503	22.916	26.659
MR = 80%										
Image (1)	22.457/0.831	20.238/0.714	23.218/0.840	22.783/0.821	27.546/0.930	23.267/0.847	23.146/0.837	22.061/0.791	23.208/0.827	27.972/0.936
Image (2)	18.554/0.621	15.330/0.368	17.766/0.524	18.540/0.550	21.838/0.777	18.296/0.586	18.882/0.590	17.867/0.482	18.911/0.550	22.659/0.788
Image (3)	21.665/0.872	20.183/0.811	22.493/0.873	22.085/0.867	28.581/0.965	22.749/0.887	22.781/0.886	21.951/0.858	23.051/0.883	29.140/0.970
Image (4)	18.554/0.760	15.574/0.617	17.920/0.727	18.535/0.751	21.800/0.868	19.093/0.778	19.066/0.774	18.299/0.729	19.255/0.778	22.331/0.884
Image (5)	18.599/0.750	15.455/0.579	17.358/0.678	18.381/0.716	21.366/0.842	18.375/0.744	18.723/0.743	18.010/0.695	18.786/0.729	21.876/0.855
Image (6)	20.996/0.885	18.637/0.772	21.429/0.878	21.309/0.874	25.655/0.948	21.725/0.892	21.638/0.886	20.883/0.869	21.756/0.884	26.045/0.951
Image (7)	19.650/0.857	17.415/0.761	20.065/0.855	20.386/0.863	25.245/0.950	19.898/0.859	20.848/0.874	19.858/0.847	21.258/0.882	25.898/0.956
Image (8)	16.947/0.767	13.941/0.578	16.013/0.703	17.006/0.758	22.177/0.898	17.239/0.776	17.407/0.770	16.160/0.709	17.461/0.764	22.177/0.908
Aver.	19.678	17.097	19.533	19.878	24.209	20.080	20.311	19.386	20.461	24.762
MR = 90%										
Image (1)	19.364/0.700	16.715/0.544	16.827/0.535	19.654/0.693	24.940/0.885	19.271/0.710	20.053/0.722	19.605/0.689	19.739/0.699	24.962/0.889
Image (2)	15.872/0.434	12.203/0.196	12.601/0.213	15.602/0.372	19.797/0.679	15.731/0.421	15.824/0.398	15.274/0.320	15.123/0.320	20.176/0.692
Image (3)	18.574/0.762	15.504/0.661	16.423/0.564	19.055/0.787	25.568/0.936	19.313/0.801	19.388/0.798	19.000/0.770	19.197/0.777	25.663/0.941
Image (4)	15.417/0.585	12.183/0.399	13.050/0.407	15.679/0.587	19.598/0.789	15.630/0.598	15.891/0.608	15.142/0.550	15.341/0.571	19.903/0.807
Image (5)	16.177/0.647	12.683/0.430	13.895/0.483	15.991/0.627	19.470/0.782	16.351/0.661	16.296/0.640	15.745/0.593	15.443/0.586	19.771/0.795
Image (6)	18.057/0.799	14.913/0.607	14.911/0.629	18.343/0.795	23.567/0.924	17.979/0.813	18.789/0.813	18.557/0.800	18.320/0.782	23.772/0.926
Image (7)	16.787/0.767	13.579/0.582	14.290/0.613	16.713/0.753	22.417/0.913	16.346/0.746	17.162/0.764	16.946/0.749	17.018/0.757	22.799/0.920
Image (8)	13.986/0.626	10.782/0.389	12.174/0.469	14.651/0.658	19.090/0.838	14.415/0.661	14.472/0.642	13.437/0.565	13.384/0.571	19.364/0.846
Aver.	16.779	13.570	14.271	16.961	21.806	16.879	17.234	16.713	16.696	22.051

(m)

Fig. 5. The completion results with MR = 70%. (a) is the original image. (b) is the observed image (MR = 70%). (c)-(l) are the completion results of IRLNM-QR, WNNM, MC-NC, TNNR, TNN-SR, LRQMC, LRQA-G, QLNF, TQLNA, and QQR-QNN-SR, respectively. (m) Quantitative quality indexes (PSNR/SSIM) of different methods.

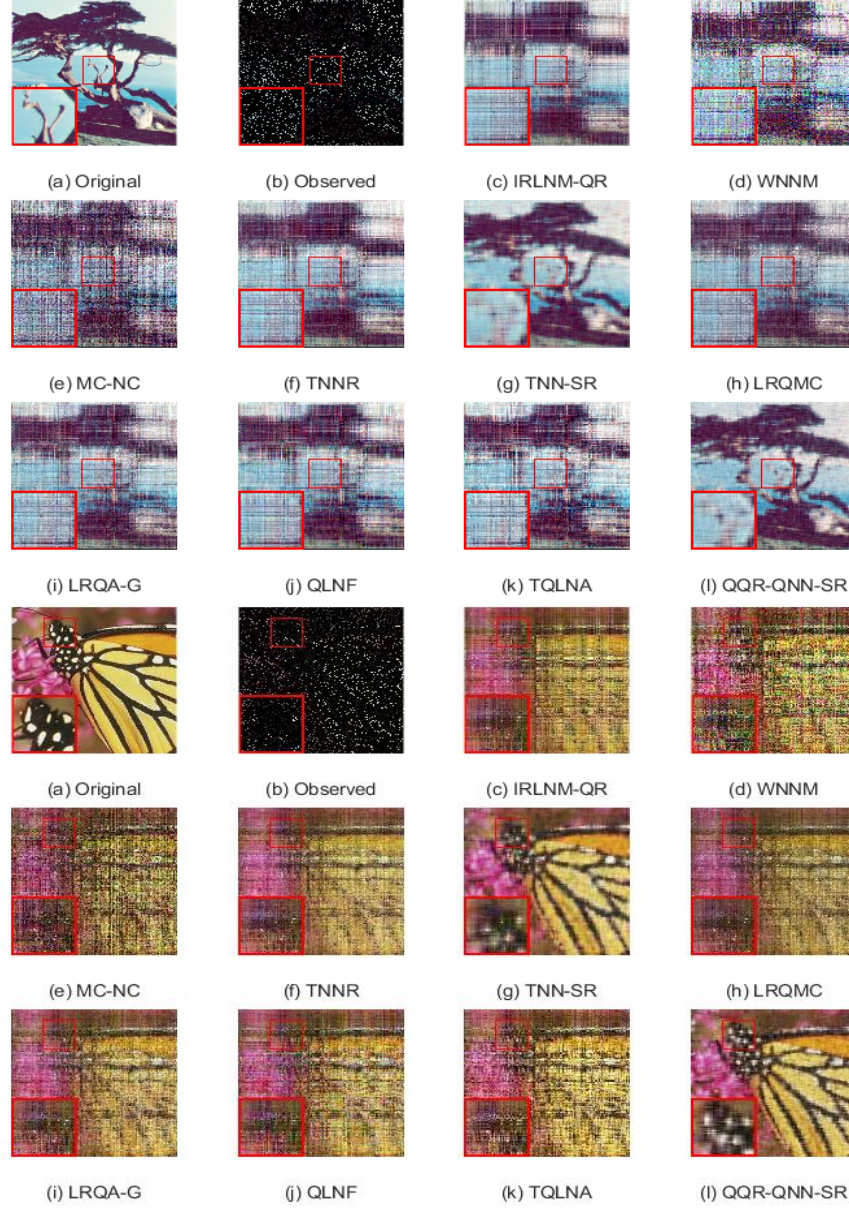
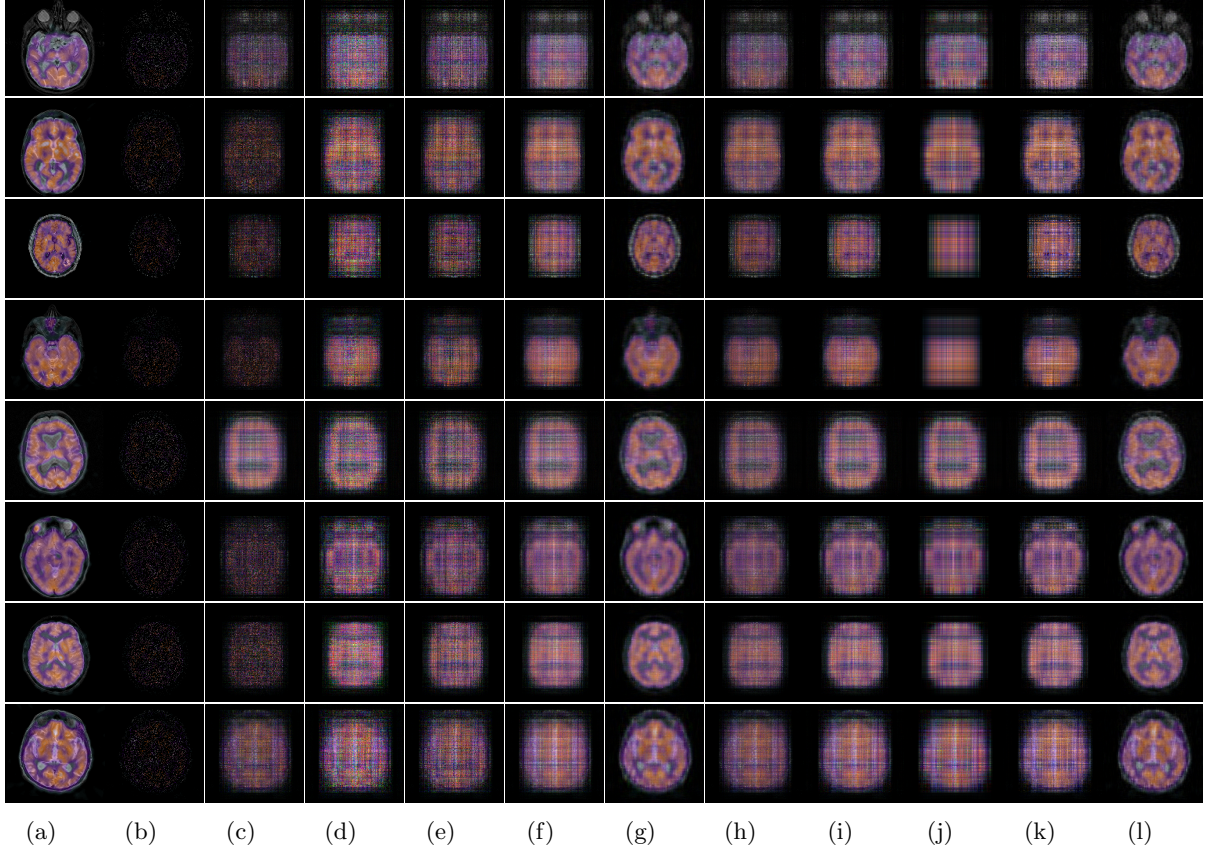


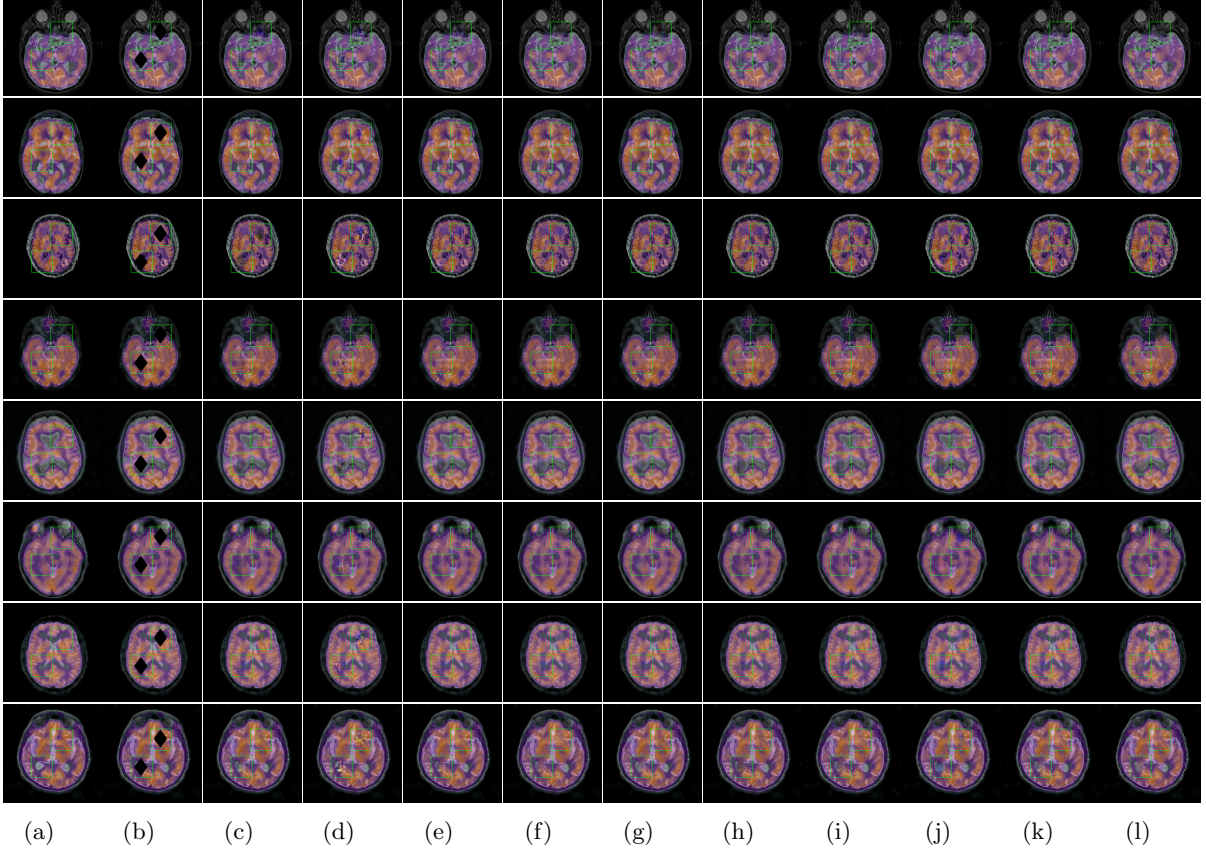
Fig. 6. The completion results with $MR = 90\%$ on Image (2) and Image (8). (a) Original image. (b) Observed image ($MR = 90\%$). (c)-(l) are the completion results of IRLNM-QR, WNNM, MC-NC, TNNR, TNN-SR, LRQMC, LRQA-G, QLNF, TQLNA, and QQR-QNN-SR, respectively.



Methods:	IRLNM-QR	WNNM	MC-NC	TNNR	TNN-SR	LRQMC	LRQA-G	QLNF	TQLNA	QQR-QNN-SR
Images:	MR = 90%									
Image (9)	15.090/0.473	13.634/0.380	15.348/0.445	17.071/0.277	21.259/0.673	17.067/0.552	17.403/0.540	17.053/0.260	16.623/0.261	21.375/0.706
Image (10)	12.624/0.501	14.347/0.528	15.719/0.562	17.541/0.499	22.202/0.692	17.861/0.632	17.755/0.629	17.523/0.500	17.208/0.512	22.366/0.733
Image (11)	15.254/0.685	14.811/0.684	16.272/0.694	17.724/0.616	20.973/0.667	17.737/0.731	17.793/ 0.733	17.511/0.588	16.659/0.609	21.014/0.724
Image (12)	14.336/0.547	17.055/0.563	18.023/0.594	20.070/0.382	24.414/0.752	19.730/0.669	20.393/0.666	18.880/0.308	20.052/0.406	24.573/0.785
Image (13)	18.235/0.564	14.861/0.387	15.918/0.489	17.947/0.298	22.672/0.741	17.534/0.572	18.334/0.580	17.977/0.303	18.273/0.354	22.989/0.761
Image (14)	13.908/0.491	15.239/0.506	16.772/0.542	18.458/0.488	23.742/0.731	18.386/0.612	18.642/0.616	18.214/0.487	18.557/0.518	24.035/0.771
Image (15)	12.978/0.545	15.982/0.557	17.022/0.585	19.168/0.549	23.627/0.743	18.764/0.659	19.346/0.654	19.179/0.546	19.539/0.572	23.715/0.780
Image (16)	15.945/0.507	13.588/0.358	15.262/0.454	16.980/0.218	21.500/0.662	16.961/0.547	17.179/0.527	16.601/0.230	16.756/0.247	21.767/0.703
Aver.	14.796	14.940	16.292	18.120	22.549	18.005	18.356	17.867	17.958	22.729

(m)

Fig. 7. (a) Original color medical images. (b) The observed color medical images (MR=90%). (c)-(l) are the completion results of IRLNM-QR, WNNM, MC-NC, TNNR, TNN-SR, LRQMC, LRQA-G, QLNF, TQLNA, and QQR-QNN-SR, respectively. (m) Quantitative quality indexes (PSNR/SSIM) of different methods on color medical images (MR=90%).



Methods:	IRLNM-QR	WNNM	MC-NC	TNNR	TNN-SR	LRQMC	LRQA-G	QLNF	TQLNA	QQR-QNN-SR
Images:	Random block missing									
Image (9)	31.268/0.988	27.331/0.982	32.451/0.989	33.237/0.836	33.004/0.989	33.049/0.990	33.283/0.990	32.957/ 0.991	32.656/0.963	33.458 /0.990
Image (10)	32.552/0.992	29.195/0.988	32.420/ 0.993	33.073/0.914	33.485/0.992	32.948/0.992	33.075/ 0.993	30.806/0.991	32.545/0.956	33.658 / 0.993
Image (11)	30.511/0.987	26.068/0.980	31.107/0.988	32.015/0.946	32.888/0.990	31.835/0.988	31.613/0.988	31.318/0.989	31.075/0.985	33.522 / 0.991
Image (12)	33.247/0.990	30.071/0.984	34.193/0.991	34.126/0.824	35.141/ 0.992	33.072/0.989	33.181/0.989	32.871/0.988	33.054/0.969	35.173 / 0.992
Image (13)	30.523/0.990	28.637/0.986	31.355/0.990	31.589/0.986	32.563/ 0.991	31.306/0.989	31.702/0.990	30.447/0.988	31.682/0.988	32.636 / 0.991
Image (14)	35.224/0.993	30.661/0.987	35.171/0.993	35.240/0.921	35.691/ 0.994	35.657/0.993	35.660/ 0.994	34.562/0.993	35.263/0.982	35.749 / 0.994
Image (15)	34.387/0.993	29.966/0.986	35.247/ 0.994	34.636/0.962	35.542/0.992	34.813/0.992	34.820/0.993	33.725/0.993	34.756/0.993	35.775 /0.993
Image (16)	29.627/0.991	26.839/0.985	29.759/0.990	30.006/0.859	31.514/ 0.992	29.847/0.988	30.158/0.989	30.432/0.990	30.194/0.980	31.907 / 0.992
Aver.	32.241	28.691	32.792	32.943	33.867	32.764	32.867	22.708	32.668	34.107

(m)

Fig. 8. (a) Original color medical images. (b) The observed color medical images (block missing). (c)-(l) are the completion results of IRLNM-QR, WNNM, MC-NC, TNNR, TNN-SR, LRQMC, LRQA-G, QLNF, TQLNA, and QQR-QNN-SR, respectively. (m) Quantitative quality indexes (PSNR/SSIM) of different methods on color medical images (2 random rhombus blocks missing).

5 Conclusions

Using quaternion matrix analysis, we proposed a new Tri-Factorization of a quaternion matrix called CQSVD-QQR, which is based on the quaternion QR decomposition and can approximate the QSVD of a quaternion matrix. The coupling between color channels may be handled naturally and the color information of color images is better retained when color pixels are regarded as vector units rather than scalars in the quaternion representation for color images. Therefore, within the context of the new quaternion matrix trifactorization, we developed a novel method for color image completion in this study, using the tool of quaternion representation of color images. Additionally, when developing the model, we take into account both the low rank of the image and the sparse prior information about the image. The method is based on CQSVD-QQR, quaternion nuclear norm, and sparse regularizer, called QQR-QNN-SR. We solve this problem under the quaternion ADMM framework. Experimental results on color images and color medical images show that the proposed method exhibits superiority in both numerical results and visual effects compared to several state-of-the-art methods.

Acknowledgments

This work was supported by University of Macau (MYRG2019-00039-FST), Science and Technology Development Fund, Macao S.A.R (FDCT/0036/2021/AGJ), and Science and Technology Planning Project of Guangzhou City, China (Grant No. 201907010043).

Declaration of competing interest

The authors declare that they have no known competing financial interests or personal relationships that could have appeared to influence the work reported in this paper.

References

- [1] Yao Hu, Debing Zhang, Jieping Ye, Xuelong Li, and Xiaofei He. Fast and accurate matrix completion via truncated nuclear norm regularization. *IEEE transactions on pattern analysis and machine intelligence*, 35(9):2117–2130, 2012.
- [2] Qing Liu, Zhihui Lai, Zongwei Zhou, Fangjun Kuang, and Zhong Jin. A truncated nuclear norm regularization method based on weighted residual error for matrix completion. *IEEE Transactions on Image Processing*, 25(1):316–330, 2015.
- [3] Shuhang Gu, Qi Xie, Deyu Meng, Wangmeng Zuo, Xiangchu Feng, and Lei Zhang. Weighted nuclear norm minimization and its applications to low level vision. *International journal of computer vision*, 121(2):183–208, 2017.
- [4] Jifei Miao and Kit Ian Kou. Color image recovery using low-rank quaternion matrix completion algorithm. *IEEE Transactions on Image Processing*, 31:190–201, 2021.
- [5] Emmanuel J Candès and Benjamin Recht. Exact matrix completion via convex optimization. *Foundations of Computational Mathematics*, 9:717–772, 2009.
- [6] Jian-Feng Cai, Emmanuel J. Candès, and Zuowei Shen. A singular value thresholding algorithm for matrix completion. *SIAM Journal on Optimization*, 20(4):1956–1982, 2010.
- [7] Kim-Chuan Toh and Sangwoon Yun. An accelerated proximal gradient algorithm for nuclear norm regularized least squares problems. *Pacific Journal of Optimization*, 6, 09 2010.
- [8] Shuhang Gu, Lei Zhang, Wangmeng Zuo, and Xiangchu Feng. Weighted nuclear norm minimization with application to image denoising. In *Proceedings of the IEEE Conference on Computer Vision and Pattern Recognition (CVPR)*, June 2014.
- [9] Feiping Nie, Heng Huang, and Chris Ding. Low-rank matrix recovery via efficient Schatten p-norm minimization. In *Proceedings of the Twenty-Sixth AAAI Conference on Artificial Intelligence*, AAAI’12, page 655–661. AAAI Press, 2012.

- [10] Lu Liu, Wei Huang, and Di-Rong Chen. Exact minimum rank approximation via schatten p -norm minimization. *Journal of Computational and Applied Mathematics*, 267:218–227, 2014.
- [11] Yuan Xie, Shuhang Gu, Yan Liu, Wangmeng Zuo, Wensheng Zhang, and Lei Zhang. Weighted schatten p -norm minimization for image denoising and background subtraction. *IEEE Transactions on Image Processing*, 25(10):4842–4857, 2016.
- [12] Xiao-Xiao Hu and Kit Ian Kou. Phase-based edge detection algorithms. *Mathematical Methods in the Applied Sciences*, 41(11):4148–4169, 2018.
- [13] Cuiming Zou, Kit Ian Kou, and Yulong Wang. Quaternion collaborative and sparse representation with application to color face recognition. *IEEE Transactions on image processing*, 25(7):3287–3302, 2016.
- [14] Yibin Yu, Yulan Zhang, and Shifang Yuan. Quaternion-based weighted nuclear norm minimization for color image denoising. *Neurocomputing*, 332:283–297, 2019.
- [15] Yongyong Chen, Xiaolin Xiao, and Yicong Zhou. Low-rank quaternion approximation for color image processing. *IEEE Transactions on Image Processing*, 29:1426–1439, 2019.
- [16] Jifei Miao and Kit Ian Kou. Quaternion-based bilinear factor matrix norm minimization for color image inpainting. *IEEE Transactions on Signal Processing*, 68:5617–5631, 2020.
- [17] Ricardo Cabral, Fernando De la Torre, João P Costeira, and Alexandre Bernardino. Unifying nuclear norm and bilinear factorization approaches for low-rank matrix decomposition. In *Proceedings of the IEEE international conference on computer vision*, pages 2488–2495, 2013.
- [18] Jianchao Yang, John Wright, Thomas S Huang, and Yi Ma. Image super-resolution via sparse representation. *IEEE transactions on image processing*, 19(11):2861–2873, 2010.
- [19] Qing Liu, Franck Davoine, Jian Yang, Ying Cui, Zhong Jin, and Fei Han. A fast and accurate matrix completion method based on qr decomposition and $l_{\{2,1\}}$ -norm minimization. *IEEE transactions on neural networks and learning systems*, 30(3):803–817, 2018.
- [20] Jing Dong, Zhichao Xue, Jian Guan, Zi-Fa Han, and Wenwu Wang. Low rank matrix completion using truncated nuclear norm and sparse regularizer. *Signal Processing: Image Communication*, 68:76–87, 2018.
- [21] Liqiao Yang, Yang Liu, and Kit Ian Kou. Quaternion optimized model with sparse regularization for color image recovery. *arXiv preprint arXiv:2204.08629*, 2022.
- [22] Patrick R Girard. *Quaternions, Clifford algebras and relativistic physics*. Springer Science & Business Media, 2007.
- [23] William Rowan Hamilton. Ii. on quaternions; or on a new system of imaginaries in algebra. *The London, Edinburgh, and Dublin Philosophical Magazine and Journal of Science*, 25(163):10–13, 1844.
- [24] Fuzhen Zhang. Quaternions and matrices of quaternions. *Linear algebra and its applications*, 251:21–57, 1997.
- [25] Musheng Wei, Ying Li, Fengxia Zhang, and Jianli Zhao. *Quaternion Matrix Computations*. Nova Science Publisher, 2018.
- [26] Wei Feng and Bo Hu. Quaternion discrete cosine transform and its application in color template matching. In *2008 Congress on Image and Signal Processing*, volume 2, pages 252–256. IEEE, 2008.
- [27] Qiaohua Liu, Sitao Ling, and Zhigang Jia. Randomized quaternion singular value decomposition for low-rank matrix approximation. *SIAM Journal on Scientific Computing*, 44(2):A870–A900, 2022.

- [28] Lu Li, Xingyu Wang, and Guoqiang Wang. Alternating direction method of multipliers for separable convex optimization of real functions in complex variables. *Mathematical Problems in Engineering*, 2015, 2015.
- [29] Mawardi Bahri, Eckhard SM Hitzer, Akihisa Hayashi, and Ryuichi Ashino. An uncertainty principle for quaternion fourier transform. *Computers & Mathematics with Applications*, 56(9):2398–2410, 2008.
- [30] Feiping Nie, Zhanxuan Hu, and Xuelong Li. Matrix completion based on non-convex low-rank approximation. *IEEE Transactions on Image Processing*, 28(5):2378–2388, 2018.